Article

Cell Reports

# The Heat Shock Response in Yeast Maintains Protein Homeostasis by Chaperoning and Replenishing Proteins

## Graphical Abstract

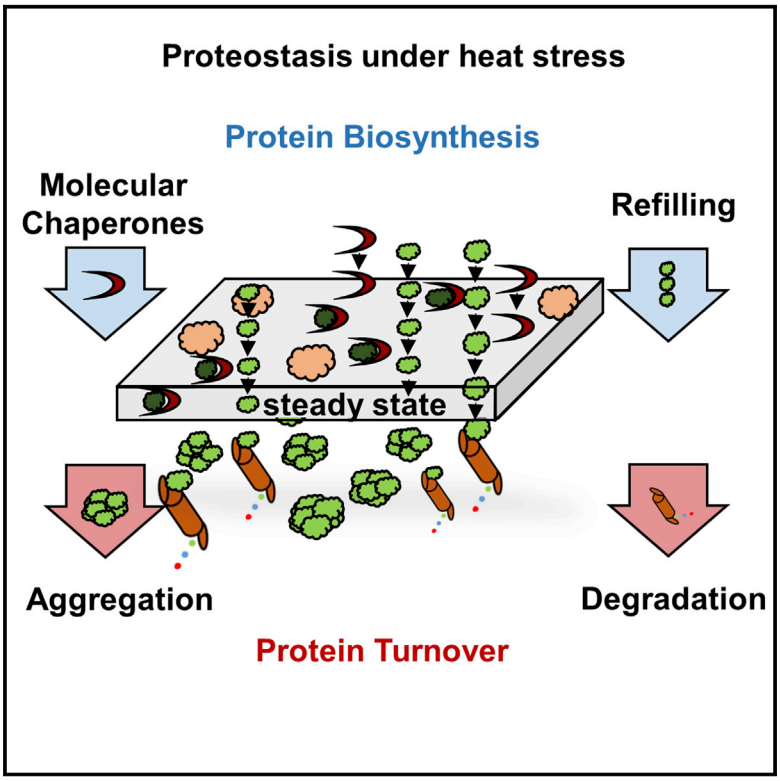


## Authors

Moritz Mühlhofer, Evi Berchtold, Chris G. Stratil, ..., Martin Haslbeck, Ralf Zimmer, Johannes Buchner

## Correspondence

johannes.buchner@tum.de

## In Brief

Mühlhofer et al. show that under mild and severe heat stress, proteins lost due to increased aggregation and degradation are replenished by increased protein synthesis to ensure a constant pool of proteins, together with the molecular chaperones. The heat shock response is activated in modules by transcriptional regulation.

## Highlights

- The HSR is modular and tuned to the severity of stress
- 90% of the upregulation under stress is required to keep protein levels constant
- Protein loss under stress is replenished by translation
- Aggregation processes shape the sublethal heat stress response

Mühlhofer et al., 2019, Cell Reports *29*, 4593–4607
December 24, 2019 
https://doi.org/10.1016/j.celrep.2019.11.109

CellPress

Cell Reports
Article



# The Heat Shock Response in Yeast Maintains Protein Homeostasis by Chaperoning and Replenishing Proteins

Moritz Mühlhofer,[1,3] Evi Berchtold,[2,3] Chris G. Stratil,[1,3,4] Gergely Csaba,[2] Elena Kunold,[1,5] Nina C. Bach,[1] Stephan A. Sieber,[1] Martin Haslbeck,[1] Ralf Zimmer,[2] and Johannes Buchner[1,6,*]

[1]Center for Integrated Protein Science at the Department of Chemistry, Technische Universität München, Lichtenbergstrasse 4, 85747 Garching, Germany

[2]Institute of Bioinformatics, Department of Informatics, Ludwig-Maximilians-Universität München, Amalienstrasse 17, 80333 Munich, Germany

[3]These authors contributed equally

[4]Present address: Boehringer Ingelheim, Fremont, Inc., 6701 Kaiser Drive, Fremont, CA 94555, USA

[5]Present address: SciLifeLab, Department of Oncology-Pathology, Karolinska Institutet, Box 1031, 171 21 Solna, Stockholm, Sweden

[6]Lead Contact

*Correspondence: johannes.buchner@tum.de

https://doi.org/10.1016/j.celrep.2019.11.109

## SUMMARY

**Life is resilient because living systems are able to respond to elevated temperatures with an ancient gene expression program called the heat shock response (HSR). In yeast, the transcription of hundreds of genes is upregulated at stress temperatures. Besides stress protection conferred by chaperones, the function of the majority of the upregulated genes under stress has remained enigmatic. We show that those genes are required to directly counterbalance increased protein turnover at stress temperatures and to maintain the metabolism. This anaplerotic reaction together with molecular chaperones allows yeast to efficiently buffer proteotoxic stress. When the capacity of this system is exhausted at extreme temperatures, aggregation processes stop translation and growth pauses. The emerging concept is that the HSR is modular with distinct programs dependent on the severity of the stress.**

## INTRODUCTION

Organisms respond to an increase in the environmental temperature with the increased expression of a set of proteins (Richter et al., 2010; Morano et al., 2012). Early studies on this heat shock response (HSR) identified a core set of strongly expressed genes, which were termed heat shock proteins (Hsps) (Lindquist, 1986; Tissières et al., 1974). Some of them are molecular chaperones, which prevent or reverse the unspecific aggregation of other proteins (Hartl et al., 2011; Lindquist and Craig, 1988; Richter et al., 2010). Temperatures only a few degrees above physiologic conditions can represent a challenge to life due to the instability of proteins, a consequence of their conformational dynamics required for function (Verghese et al., 2012). Concepts explaining the HSR have focused mainly on molecular chaperones. However, global approaches analyzing the HSR in yeast revealed that many more than only the *hsp* genes are differentially regulated (Gasch et al., 2000; Eisen et al., 1998; Liu et al., 2016; Jarnuczak et al., 2018; Gerashchenko and Gladyshev, 2014; Gerashchenko et al., 2012). Recently, besides regulation at the transcriptional level, phase transition of specific RNA-binding proteins, such as PAB1 or PUB1, was suggested to be involved in regulating the HSR in yeast (Kroschwald et al., 2018; Riback et al., 2017; Wallace et al., 2015).

Despite the discovery of HSR decades ago and recent progress, our understanding of the HSR is still sketchy. To obtain a comprehensive picture that explains the upregulation of the enigmatic roughly 90% of heat-induced genes, we analyzed the HSR by transcriptomics, translatomics, and proteomics from mild (37°C), severe (42°C), to sublethal stress (46°C) in yeast. Our results reveal that the majority of upregulated genes are required to maintain proteostasis by directly balancing increased stress-dependent protein aggregation and degradation processes. The response is specific for the severity of the stress.

## RESULTS

### Kinetic Analysis of Transcriptome Changes under Heat Shock Conditions

We investigated the reprogramming of yeast cells upon heat stress in a quantitative and kinetic manner by time-resolved transcriptome analyses for three heat shock conditions (Figures 1A, 1B, and S1A). Under mild heat shock conditions (37°C), the change in gene expression peaks within the first 15 min, with roughly 1,800 significantly changed genes. At severe heat shock conditions (42°C), up to ~3,100 genes exhibited a changed expression profile (Figure 1A). Notably, the total amount of mRNAs does not seem to change substantially (Figure S1C) compared to non-stress conditions (Miura et al., 2008).

The kinetics of the HSR are strikingly different depending on the severity of the stress. At 37°C, after an initial burst, the

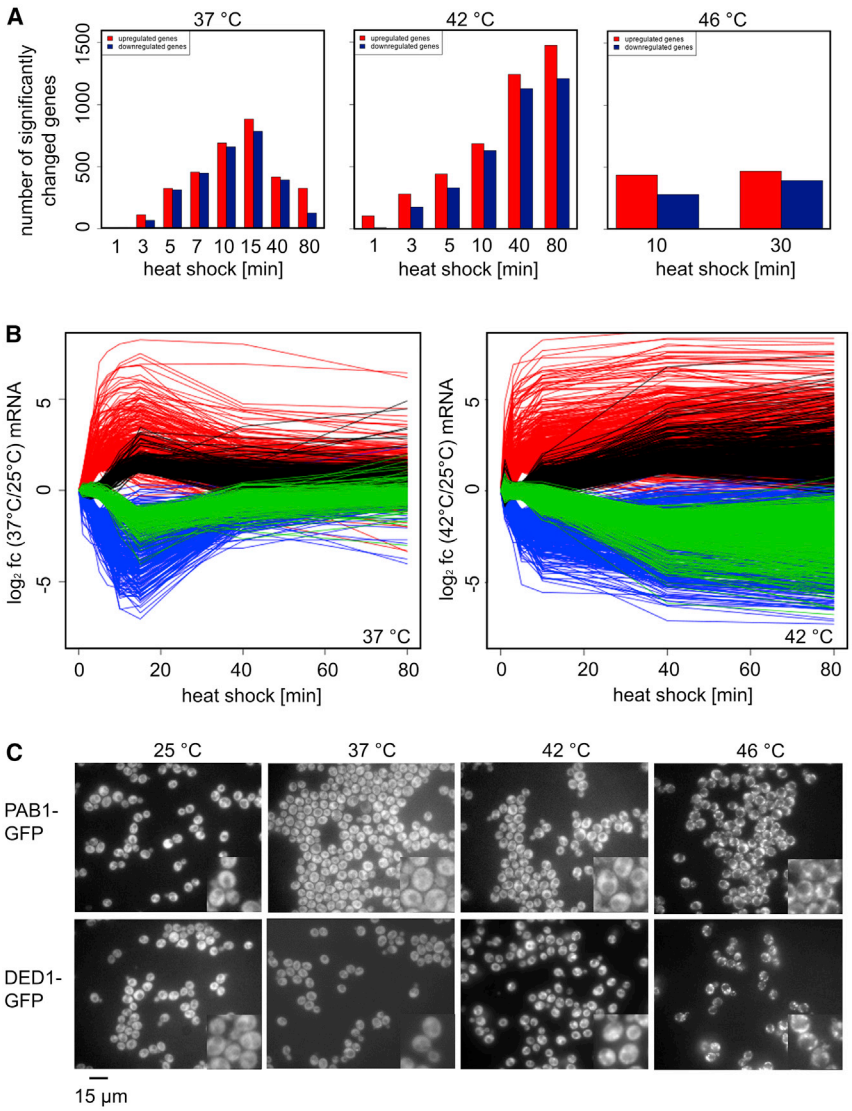


**Figure 1. The Transcriptomic HSR Is Fast and Involves Hundreds of Genes**

(A) Bar plot of the changed genes in the microarray transcriptome analysis. Number of significantly changed genes at 37°C (left), 42°C (middle), and 46°C (right). Cells were stressed for 80 min (30 min at 46°C) and samples taken at the indicated time points. The transcriptomes were analyzed with microarrays (Yeast Genome 2.0; Affymetrix) in biological duplicates or triplicates. mRNA levels were considered to be changed if $|\log_2$ fold change (fc)$| >$ 1 and $p < 0.05$ for at least one time point. Upregulated genes are shown as red bars, and downregulated genes as blue bars. Comparisons of RNA-seq and microarrays as well as the responses at the different temperatures are shown in Figures S1A and S1B.

(B) Kinetic analysis of the transcriptomic HSR at 37°C (left) and 42°C (right) for up to 80 min. Genes were grouped into early up (red), late up (black), early down (blue), and late down (green). 37°C: for early upregulation, a $\log_2$ fc of at least 1 at 5 min was assumed, along with an increase of at least 0.3 between 1–5 min, respectively. Late upregulation was defined as an absolute $\log_2$ fc below 0.5 during the initial 10 min and a $\log_2$ fc above 1 at 10/15 min. For downregulation, negative values with the same criteria as for upregulation were applied. 42°C: for early up genes, a $\log_2$ fc >0 at 3 min and >1 at 5 min was required. For late upregulation, $\log_2$ fc <0.5 up to 5 min and >1 at 10/40 min was set. For downregulation, the respective negative values were applied.

(C) PAB1 and DED1 foci formation *in vivo*. Cells with GFP-tagged PAB1 or DED1 were grown at 25°C in YPD until an optical density 595 ($OD_{595}$) of 0.8 was reached. The cells were stressed for 30 min at 37°C, 42°C, or 46°C. Foci formation was analyzed under the microscope at a magnification of 1,600×. The scale bar represents 15 µm. Insets: represent close ups of cells at a magnification of 3,200×.

HSR decreases, whereas at 42°C the HSR further increases over time. These differences reflect the success of the reprogramming at 37°C where the transient changes in expression suffice to adapt to the new conditions. However, at 42°C, the negative consequences of stress cannot be balanced completely and the stress response continues. At sublethal stress (46°C), less than 1,000 genes changed expression levels and the HSR is maintained to guarantee survival.

The upregulated genes belong to several Gene Ontology (GO) categories with response to heat, oligosaccharide metabolism, protein folding, and protein catabolic processes as the most significantly enriched ones. They include the stress-responsive molecular chaperones as well as the biosynthesis enzymes for trehalose, a stress-protective sugar (Conlin and Nelson, 2007; Gibney et al., 2015). In addition, detoxification reactions are upregulated, including peroxisomal and vacuolar processes. By comparing the upregulated genes at the different temperatures, a modular fashion of the HSR becomes visible (Figure S1B). The first module, genes upregulated only at 37°C, comprises mostly genes annotated to membrane and to mitochondria. There is a large overlap with 42°C, including genes involved in autophagic processes as well as ubiquitin conjugation. Additionally, at 42°C, sporulation is upregulated, consistent with the idea that cells prepare for dormancy to ensure survival. The overlap between the mild and sublethal HSR comprises only a few genes, supporting the idea of a stepwise activation of the HSR with increasing temperatures. At prolonged severe stress, autophagy becomes important. The core module of the HSR, which covers genes that are upregulated at all temperatures, includes 286 genes after 10 min and 163 genes after prolonged heat stress. GO analysis identified stress response, ubiquitin conjugation, and glycolysis, as the affected key processes (Figure S1B). Detailed kinetic analyses of the transcriptomic responses at 37°C and 42°C revealed that the HSR is rapid, with a large number of changes seen within the first minutes (Figure 1B). The kinetics of the changes in expression span a wide range, whereas,

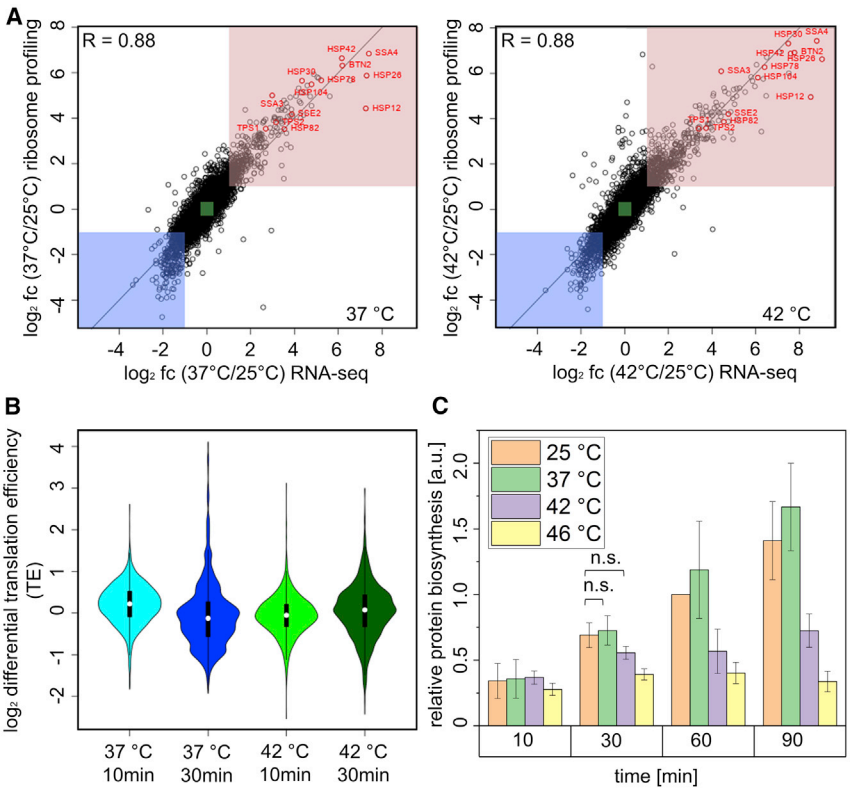


**Figure 2. Regulation at the mRNA Level Is Directly Conferrable to Differential Ribosomal Occupancy**

(A) Analysis of the translational HSR of *S. cerevisiae* by ribosome profiling. Logarithmic growing yeast cultures were heat stressed at 37°C and 42°C for 10 min. Experiments were conducted in biological duplicates or triplicates. RP $\log_2$ fcs were scattered against $\log_2$ fcs of the corresponding RNA-seq experiment of the same sample. Selected heat shock related genes are indicated in red (R, Pearson correlation). The red box highlights upregulated genes at the mRNA and translational level, the green box unchanged genes ($|\log_2 fc| < 0.3$), and the blue box genes that are downregulated at the mRNA and translational level. Genes with $\log_2$ changes between 0.3 and 1 represent a gray area and were neither grouped as upregulated nor as unchanged. The comparisons after 30 min of heat stress are shown in Figure S2A.

(B) Changes in translational efficiency (TE). TE was calculated by dividing the ribosome protected fragment reads by the mean RNA-seq reads after median normalization. The differential TE is the fc between the TEs of stressed and control conditions. A more detailed ribosomal occupancy analysis is shown in Figures S2B and S2C.

(C) *De novo* translation under stress was investigated by $^{35}$S-methionine incorporation. Cells were stressed at the indicated temperatures for 90 min. At each time point, at least biological duplicates were measured. Both 30-min and 60-min stress samples (37°C and 42°C) were measured in biological triplicates. Densitometric analysis was performed with ImageQuantTL. Every dataset was normalized to protein biosynthesis after 60 min at 25°C. The bar plot shows mean values ± SD. Changes after 30 min are not significant according to a two-sample t test ($p < 0.05$). The corresponding gel is shown in Figure S2D.

e.g., the levels of *hsp26* transcripts increase 158-fold within 5 min at 42°C, and *osw1* levels (coding for a protein involved in sporulation) stay completely unchanged within the first 5 min and then steadily increase up to 68-fold after 80 min. Molecular chaperones and trehalose metabolism enzymes are upregulated fast. In the late-upregulated group are mostly proteins involved in metabolic processes at 37°C, whereas at 42°C, protein degradation is upregulated with time.

GO analyses of the downregulated genes unambiguously pinpoint translation as well as ribosome biogenesis. However, the rRNA levels stay constant. Thus, the overall number of ribosomes does not drop substantially (Figure S1D).

Importantly, of the upregulated genes after 10 min at 37°C and 42°C, only approximately 4% are annotated with protein folding (Figure S1A; red areas). To understand the cell's effort to regulate more than 1,000 additional genes differentially whose function under stress is completely unclear, we investigated translation during the HSR.

## mRNAs Are Quantitatively Translated into Proteins

As phase transition and stress granule formation are known to affect translation initiation (Protter and Parker, 2016; Itakura et al., 2018), we first analyzed the stress-dependent aggregation of GFP-tagged RNA helicase DED1 and polyA-binding protein PAB1 *in vivo* (Cherkasov et al., 2015; Riback et al., 2017; Wallace et al., 2015). At 37°C, DED1 stayed soluble, whereas at 42°C, in some cells DED1 foci were formed (Figure 1C). This indicates that at temperatures around 42°C, DED1 aggregation sets in. A further increase of the temperature to 46°C led to foci formation in all cells tested, in agreement with previous analyses (Cherkasov et al., 2015). PAB1, a potential thermosensor for the HSR in yeast (Riback et al., 2017; Wallace et al., 2015), stayed soluble up to 42°C. Incubation at 46°C led to the complete aggregation of PAB1, as shown before (Cherkasov et al., 2015; Wallace et al., 2015). Thus, we expect effects on translation to occur mainly at temperatures above 42°C.

To investigate whether all the heat-shock-induced mRNAs are indeed translated at temperatures up to 42°C, ribosome profiling was applied (Ingolia et al., 2012). We identified more than 1,000 mRNAs whose ribosomal occupancy was elevated under stress and several hundred transcripts whose ribosome-protected fragment reads were strongly reduced. For both 37°C and 42°C, good to excellent correlations (Pearson values from 0.73–0.92) between changes in transcription and ribosomal occupancy of the mRNAs were observed (Figures 2A and S2A). Thus, the changes in transcription during the HSR appear to result in equivalent changes in translation.

Subsequently, we determined the translation efficiency (TE), which is calculated by dividing the ribosome-protected fragment reads through the mean RNA reads of the corresponding RNA sequencing (RNA-seq) experiment (Ingolia et al., 2009). Compared to 10 min at 37°C, the TE decreased slightly after

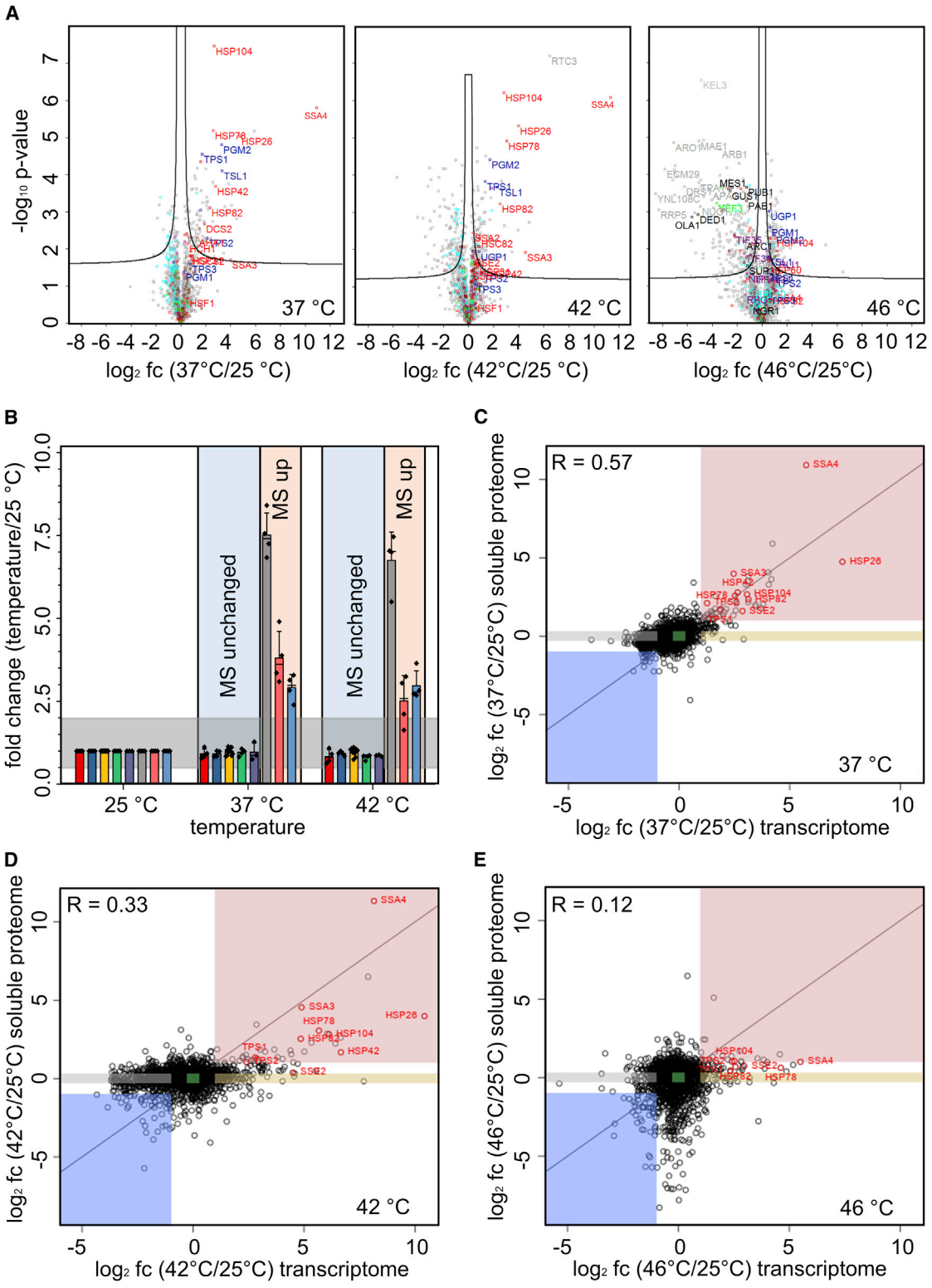


**Figure 3. Transcriptomic and Proteomic Heat Stress Response Do Not Correlate Well**

(A) For proteomic analysis, logarithmic cells were heat stressed for 30 min and the relative changes in the soluble protein fraction measured by label-free quantitative mass spectrometry (LFQ-MS). For the volcano plots, a two-sample t test with false discovery rate (FDR) < 0.05 was applied. As a control, the soluble protein fraction of unstressed *S. cerevisiae* was used. All proteomic measurements were conducted in biological triplicates. Proteins that, according to the

*(legend continued on next page)*

longer exposure to 37°C. At 42°C, the TE was marginally reduced throughout the whole measurement (Figure 2B). Thus, we conclude that protein biosynthesis is maintained under stress. Even though the global effect was small, we also determined the TEs of individual mRNAs by analyzing the distribution of the ribosomes over the length of the transcripts (Figure S2B). In non-stressed cells the ribosomes are distributed almost equally across the mRNAs, whereas in heat-stressed cells they tend to accumulate at the beginning of the transcripts, supposedly due to impaired elongation (Figure S2B), as observed in mammalian cells (Shalgi et al., 2013). Similarly, we found that ribosome pausing is closely linked to the presence of hydrophobic amino acid patches (Figure S2C). Nevertheless, within 30 min at 37°C and 42°C, translation of only a subset of genes is partially repressed. At 37°C, the effect decreased over time, whereas at 42°C the small stalling effect was perpetuated. Thus, also in the ribosome occupancy profiles, the adaption to mild heat stress, observed in our transcriptome analysis, is recapitulated. The finding that translation is largely pursued up to 42°C is in excellent agreement with the onset of aggregation of translation factors at ~42°C in the microscopic studies (Figure 1C).

To monitor *de novo* protein biosynthesis directly, we used a pulse labeling approach in which we incorporated $^{35}$S-methionine into proteins. Quantitative analysis of the radiolabeled proteins showed that translation was not significantly decreased within the first 30 min at 42°C (Figure 2C; Figure S2D). However, upon prolonged stress at 42°C, *de novo* protein synthesis was affected, indicating a regulated shutdown. Unexpectedly, at 37°C, *de novo* protein synthesis was slightly higher than that under non heat shock (NHS) conditions. Importantly at 46°C, translation ceased after 10 min and the stop of translation was maintained even during 90 min of recovery, whereas at 42°C, translation slowly resumed during recovery (Figure S2E).

We conclude that aggregation does not play a major role in regulating the induction or maintenance of the HSR in *Saccharomyces cerevisiae* at temperatures up to 42°C. Rather, it represents a regulatory checkpoint at more severe and prolonged heat stress conditions, leading to the shutdown of translation. Thus, the regulation at the mRNA level is reflected in the translational profile under stress.

## Proteome Changes under Heat Shock Do Not Correlate with Gene Regulation

To determine differences at the proteomic level during the HSR, we performed fractionated (soluble/insoluble/total) label-free quantification mass spectrometry (LFQ-MS). In these experiments, we identified 1,857 soluble proteins after 30 min at 37°C or 42°C. At 37°C, 10 proteins were significantly downregulated, whereas 63 proteins were significantly upregulated ($|\log_2$ fold change [fc]$| > 1$; false discovery rate [FDR] $< 0.05$; $S_0 = 0.1$) compared to non-stressed cells (Figure 3A). At 42°C, 54 significantly upregulated proteins face 92 significantly downregulated ones. Thus, especially the number of downregulated proteins was increased under more severe stress. This was also visible at 46°C where almost 1,800 proteins were detected in the soluble fraction after 30 min. Here, 47 proteins were found to be significantly upregulated and 220 proteins were significantly downregulated. Among the upregulated proteins at 37°C and 42°C, we found chaperones (e.g., SSA3/4, HSP26, HSP42, HSP82, and HSP104), proteins involved in trehalose metabolism (HXK1, TPS1, TPS2, TSL1, and NTH1), as well as proteins involved in glycerol metabolism (e.g., GCY1 and ALD3) (Figure 3A). Besides trehalose, glycerol is also known to confer stress resistance in yeast (Conlin and Nelson, 2007; Gibney et al., 2015; Klein et al., 2017).

Surprisingly, the proteome changes upon stress did not correlate well with those observed in transcription, especially at higher temperatures (Figures 3C–3E). Many genes that were differentially regulated at the transcriptional level remained constant at the protein level. At 37°C, the correlation between the transcriptome and proteome improved over time as the cells adapt to the stress and the transcriptomic changes are smaller compared to earlier time points (R = 0.57; Figure 3C). At severe stress, the correlation between the transcriptome and the proteome was poor (42°C; R = 0.33; Figure 3D). We defined five different regulatory categories: only a small number of proteins are upregulated

Uniprot GO BP annotation (2015), categorized in response to heat are colored red, trehalose biosynthesis blue, translation in cyan, translation initiation in purple, translation elongation in green, and ubiquitin-dependent catabolic process in brown. Known phase separators were colored in black in the volcano plot corresponding to the 46°C measurement. Targeted metabolic pathways at mild and severe stress are shown in Figure S3.

(B) Lysates of heat stressed cells were analyzed by western blot to validate the MS results. Fcs were calculated by dividing the band intensity at the respective (stress) temperature by the band intensity at 25°C. In the bar plot, the mean values (bar height), median (black line), and the standard deviation are shown. For each protein, at least 3 biological replicates were measured. Five proteins that were not upregulated in the MS measurement (blue box) were tested. Red: CMK2, blue: TDH1, yellow: PGK1, green: CNB1, purple: HCH1. Furthermore, three proteins that were upregulated in the MS measurement (red box) were tested. Gray: HSP26, light red: HSP42, light blue: HSP104. The gray box indicates the fc range from 0.5 to 2, in which we assume proteins neither to be down- nor to be upregulated. The corresponding western blots are shown in Figure S4A. CMK2 was hemagglutinin (HA) tagged and, therefore, detected with an anti-HA antibody.

(C) Comparison of the transcriptome from two biological replicates and the soluble proteome (three biological replicates) of heat stressed yeast after 30 min at 37°C. The red box highlights actively upregulated proteins ($\log_2$ fc $> 1$ at the mRNA and proteomic level). Orange box: Proteins whose levels are actively kept constant by upregulated transcription ($\log_2$ fc $> 1$ at the mRNA and $|\log_2$ fc$| < 0.3$ at the proteomic level). Green box: proteins whose levels are passively kept constant ($|\log_2$ fc$| < 0.3$ at the mRNA and proteomic level). Gray box: proteins with increased stability that allows transcriptional downregulation with no change at the proteome level ($\log_2$ fc $< -1$ at the mRNA and $|\log_2$ fc$| < 0.3$ at the proteomic level). Blue box: actively downregulated proteins ($\log_2$ fc $< 1$ at the mRNA and proteomic level). Genes/proteins with changes between 0.3 and 1 were grouped neither as regulated nor as unchanged and, therefore, are unboxed. Selected upregulated heat stress related genes/proteins are colored red (R, Pearson correlation). Corresponding 2D enrichment analysis is shown in Figure S4B.

(D) Comparison of the transcriptome from two biological replicates and the soluble proteome (three biological replicates) of heat stressed yeast after 30 min at 42°C. The color code is the same as in (C). Corresponding 2D enrichment analysis is shown in Figure S4C (R, Pearson correlation).

(E) Comparison of the soluble proteome after 30 min at 46°C (biological triplicates) with the corresponding transcriptome (biological duplicates) measurement. The color code is the same as in (C) (R, Pearson correlation).

(red box) and even less that are downregulated (blue box) at both levels. Many genes/proteins stay unchanged (green box), whereas others, especially at 42°C, were actively kept constant at the protein level by upregulating the respective mRNA (orange box). In the fifth group, relatively stable proteins were identified that maintained their levels even though the respective mRNAs were downregulated (gray box). The results obtained by LFQ-MS were validated with western blots (Figures 3B and S4A). We selected five proteins that were not upregulated at the protein level under stress and three proteins that were upregulated (Figures 3B and S4A). All of the tested proteins behaved as it was expected from the MS measurement.

To obtain a clearer picture of the processes involved in the HSR, we only considered the fc ($|\log_2 fc| > 1$) to increase the number of changed proteins. At 37°C, we found that in addition to orchestrating stress resistance mechanisms, specific metabolic processes are targeted by the HSR. With hexokinase (HXK1) and pyruvate kinase (PYK2), two of the three key enzymes of glycolysis are upregulated as well as several enzymes of the glycogen metabolism, pyruvate turnover to citrate or 1,4-butanediol, and the clearance of the toxic glycolysis side product methylglyoxylate (Figure S3).

At 42°C, carbohydrate metabolic pathways (glycogen and pyruvate) seem to become less important, whereas more proteins involved in regulating cell cycle and division were found to be upregulated. At both temperatures, ribosomal proteins and proteins involved in translation were downregulated. At 37°C, 28 proteins sort into this category. At 42°C, 50 downregulated proteins are involved in translation, consistent with the decrease in translation observed in the pulse chase experiments under prolonged stress (Figure 2C). However, translation initiation factors stay mostly unchanged, which supports our ribosome profiling results. Under both stress conditions, we observed a downregulation of three of the six enzymes involved in diphthamide biosynthesis (DPH1, JJJ3, and RRT2). Diphthamide is a modified histidine residue of elongation factor eEF2, which enhances translation fidelity (Schaffrath and Stark, 2014). Hence, the downregulation of those enzymes goes in line with a specific translational shutdown during prolonged heat stress (Figure S3).

The conspicuous GO categories at the translatome level at 37°C and 42°C are chaperones, trehalose, vacuolar catabolic process, autophagy, monosaccharide metabolism, and respiratory electron chain. We analyzed how many upregulated proteins sort into these processes and found that all categories but respiratory electron chain, autophagy, and, at 37°C, monosaccharide metabolism were significantly enriched for the upregulated proteins (Figure 4A). The number of upregulated metabolic enzymes was higher at 37°C compared to 42°C, which is in line with our observation that at mild heat stress growth is unaffected. At 37°C, vacuolar degradation processes seem to be more dominant, whereas at 42°C, autophagic processes gain importance.

When we focus on the group of proteins whose levels are kept constant by upregulated translation and sort them into the same categories, it becomes visible that at 37°C almost no proteins distributed into the selected GO terms. Also at 42°C, only a few proteins of those groups were found to be unchanged even though their translation was increased (Figure 4B). This indicates that the main stress protective pathways are also upregulated at the protein level. The 2D enrichment analysis further supported that the main categories targeted by translatomic and proteomic response overlap and correlate at 37°C (R = 0.72; Figure S4B) and 42°C (R = 0.78; Figure S4C). Apparently, for less stable proteins, transcriptomic upregulation is needed to maintain the protein level and keep metabolic processes active. Hence, the regulation on the mRNA level has to be more extensive at 42°C.

At 46°C, however, the targeted pathways are less clear. Hsps and trehalose enzymes are still upregulated but not nearly to the same extent as at lower temperatures. This is consistent with our finding that protein synthesis is suppressed, and Hsps are not excluded from the effect. Known phase separators such as PAB1, PUB1, DED1, MES1, GUS,1 or OLA1 were all found to be significantly downregulated in the soluble fraction (Figure 3A), as expected (Wallace et al., 2015). Hence, translation and, especially, translation initiation are negatively affected by the sublethal stress. Nevertheless, translation elongation and termination factors were mostly unchanged. Furthermore, ubiquitin-dependent protein degradation, which was upregulated at 37°C and 42°C, was not found to be increased at sublethal stress. This indicates that at 46°C, aggregation processes mainly shape the stress response.

There is almost no correlation between the transcriptome and the proteome at 46°C (R = 0.12; Figure 3E). The fast upregulation of genes at the mRNA level did not result in equally changed protein levels, as translation stopped at 46°C. Furthermore, the aggregation processes, which lead to strong protein depletion in the supernatant, are not replenished by transcription. In summary, the discrepancy between transcriptome and proteome at 46°C can be explained by a shutdown of translation and elevated protein aggregation. However, the reason for the bad correlation at lower stress temperatures (Figures 3C and 3D) remained mostly unclear.

## Modeling the HSR

In view of the bad correlation between the transcriptome/translatome and the proteome, aggregation, degradation, and impaired translation are possible processes that might explain the missing upregulation of proteins despite increased transcription. Nevertheless, these processes cannot explain why many proteins with a downregulated transcript level are not downregulated on the protein level. Previously, a dynamic mathematical model had been set up in the context of osmotic stress to describe the protein change over time as a function of absolute protein and mRNA amounts, protein half-life, mRNA change, and organismic growth (Lee et al., 2011). In this model, a significant downregulation of hundreds of proteins is unlikely, as the protein copy number per cell and the half-lives are much higher than the copy number and the half-lives of the respective mRNAs (Kulak et al., 2014; Miura et al., 2008; Belle et al., 2006; Geisberg et al., 2014; Ghaemmaghami et al., 2003). It was argued that the constant protein level of downregulated genes is due to the growth arrest at higher salt concentrations. However, for the HSR, this scenario does not fit, as only cells that were heat shocked at 46°C showed a phenotype, differing from the non-stressed cells, and did not grow anymore (Figures S5A and S5B). At 42°C and below, the phenotype of the cells did not differ from the

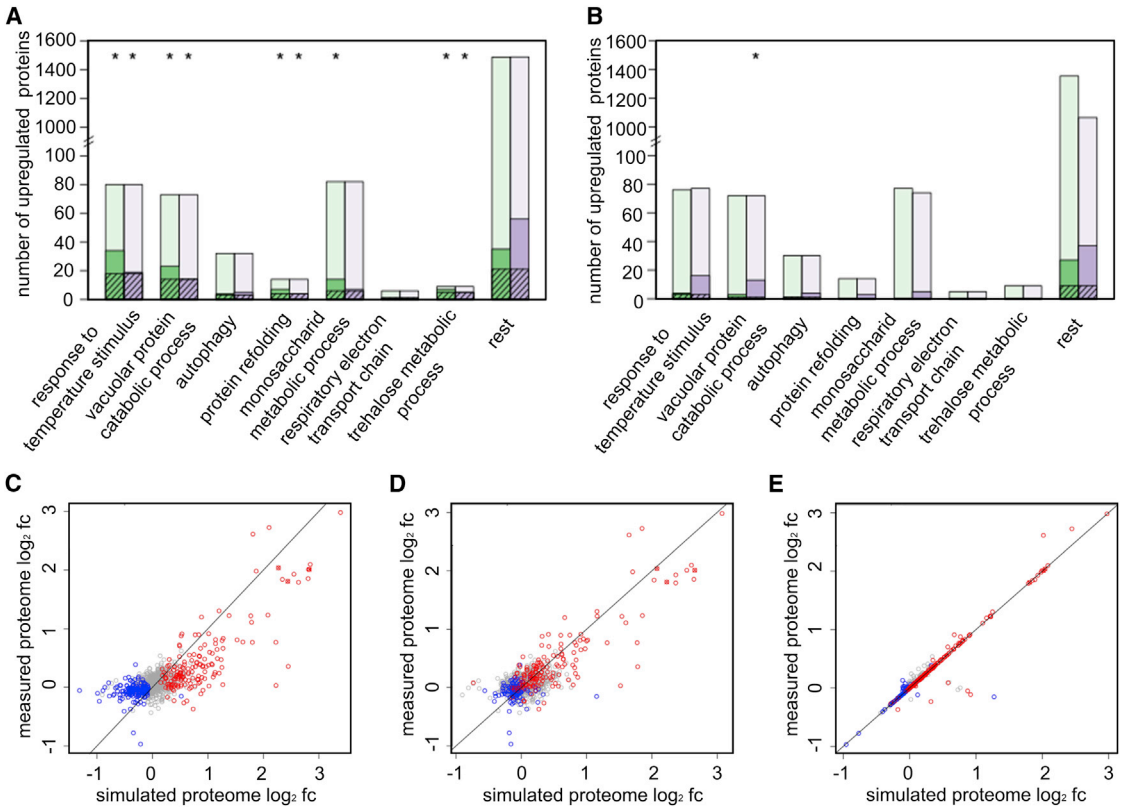


**Figure 4. Core Pathways and Mathematical Model of the HSR**

(A) Proteins that were found to be upregulated ($\log_2$ fc > 1) in the LFQ-MS measurement were clustered according to the targeted GO terms at the translational level (Huang et al., 2009). Green bars: 37°C, purple: 42°C. Black-striped parts of the bars indicate the number of proteins that were upregulated under both conditions. Faded parts of the bars indicate the total number of measured genes in the respective group. Asterisk indicates processes that are also enriched at the proteomic level.

(B) Proteins that were found to be upregulated ($\log_2$ fc > 1) at the translational level and unchanged in the LFQ-MS ($|\log_2 \text{fc}| < 0.3$) were grouped into the indicated categories. The color code is the same as in (A). Asterisk indicates processes that are also enriched for unchanged proteins with upregulated translation.

(C–E) Modeling of the protein changes during heat shock. Comparison of measured and simulated protein fcs after 30 min when steady-state half-lives are used (no parameters optimized; C). Comparison of measured and simulated protein fcs when a multiplicative factor is applied to the half-lives of the proteins that are up- (red) or downregulated (blue) in the ribosome profiling data (2 parameters optimized; D). Comparison of measured and simulated protein fcs when for each protein an individual half-life is fitted (one parameter per protein optimized; E). Further modeling approaches are shown in Figure S5C–S5F.

non-stressed cells, and we did not observe a growth arrest. Moreover, we do not have to fit the translation rates, as they were directly derived from ribosome profiling. However, when we incorporated our data into the dynamic modeling approach, we were still not able to obtain satisfying correlations of the prediction with the measured changes (Figure 4C). Thus, growth, NHS protein half-lives, protein synthesis rates, and absolute mRNA as well as protein amounts do not suffice to explain the observed small protein changes.

It is reasonable to assume that increased temperature has specific effects on the stability of individual proteins. To model this, we defined three groups of proteins with modified half-lives to account for changes in the soluble protein fraction, e.g., due to aggregation and degradation, namely, proteins with unchanged stability, proteins that become less stable, and proteins that become more stable (i.e., due to protection by chaperones). For the two groups with altered stability, we optimized one factor each that is applied to their steady-state half-lives (2-parameter model). The optimization yields ~50% reduced half-lives of the upregulated genes and ~70% increased half-lives for the downregulated genes, which substantially improved the ability of the model to predict the measured protein fcs (Figure 4D). As the resulting fit was still not perfect, we included individual protein half-lives (as the sum of aggregation and degradation) that further improved the correlation between the model and the experimental data (Figure 4E). Instead of optimizing individual protein half-lives (one parameter per protein), one can also assume that there are mechanisms influencing the TE to optimize an individual protein synthesis rate (Figures S5C–S5F). This yields a fit comparable to that when the protein half-lives are optimized individually. Thus, combining all previous experimental observations, we were able to design a mathematical model for the HSR of *S. cerevisiae*. This model strongly indicates that the loss of stability of individual proteins is affected to different degrees. This is balanced by the HSR to maintain protein levels. We, therefore, analyzed protein fate under heat stress experimentally.

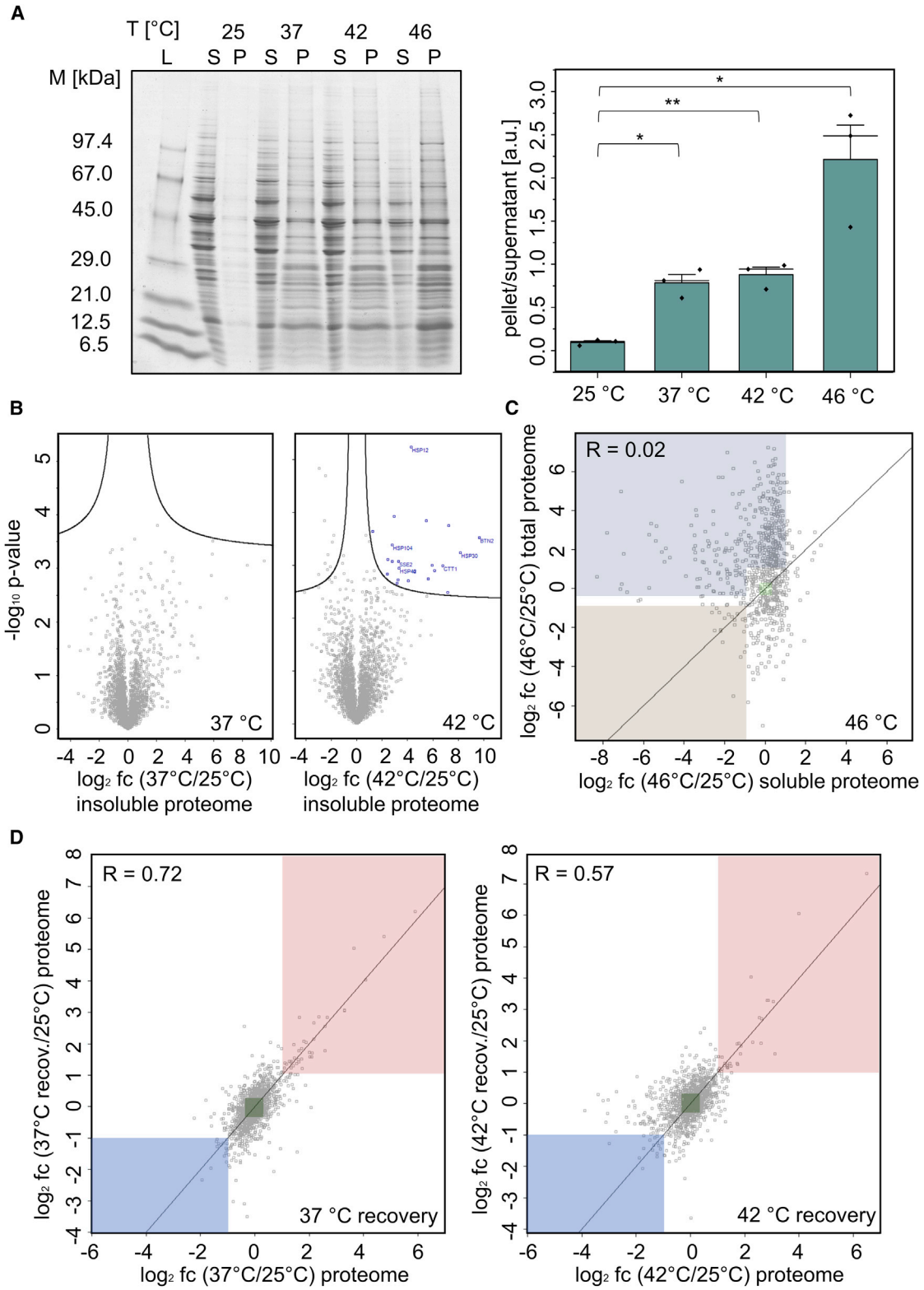


**Figure 5. Severe and Sublethal Stress Lead to Significant Aggregation Processes**

(A) Pellet and soluble fractions of yeast protein extracts collected after 30 min at the respective heat stress temperatures were analyzed by SDS-PAGE and evaluated densitometrically. On the left, a representative gel is shown. The mean value, standard deviation, and the median (black line) of three measurements are shown in the bar plot on the right. Two-sample t tests were performed to estimate the significance (N.s.: $p > 0.05$; *$p < 0.05$; **$p < 0.01$) of the changes.

*(legend continued on next page)*

### Stronger Expression Compensates Protein Aggregation under Heat Shock

Our data suggest that upregulation on the mRNA level is necessary to increase the levels of stress-protective proteins, such as molecular chaperones, and to directly compensate aggregation/turnover to ensure a constant pool of soluble proteins. To control how many proteins are aggregating in our experimental setup at 37°C or 42°C, we quantified the proteins in the insoluble pellet by LFQ-MS. Even though the pellet fraction was slightly increased, we observed no statistically significant aggregation of single proteins at 37°C (Figures 5A and 5B). However, at 42°C, 22 aggregating proteins were identified in the LFQ-MS analysis (Figure 5B). Analysis of proteins that were enriched in the pellet fraction revealed components of the protein folding machinery, e.g., HSP42, BTN2, and HSP104, which are known to be involved in the formation and dissolution of intracellular aggregates (Alberti, 2012; Grousl et al., 2018; Miller et al., 2015). Consistent with our microscopic analysis, known phase separators, such as PAB1, or DED1 stayed unchanged or were only slightly increased in the pelleted fraction at 42°C. When the soluble and the total protein fractions of the cells stressed at 46°C are compared, it becomes apparent that at 46°C aggregation and not degradation is the main reason for the depletion of the soluble proteins (Figure 5C). Most of the proteins that decreased in the soluble fraction stay constant or are even increased in the total fraction. Additionally, many proteins that are unchanged in the soluble fraction are increased in the total proteome fraction, which also indicates aggregation processes. Summarizing, aggregation processes seem to be more important at higher temperatures, whereas at 37°C, aggregation is not a key factor.

### The Proteomic Response Is Slightly Delayed under Severe Stress

To cover the dynamic range of the changes at the protein level, we shifted the cells stressed at 37°C and 42°C back to the permissive temperature (25°C) after heat stress. LFQ-MS analysis showed that the proteome of the recovered cells was similar to the proteome of cells kept at 37°C. This indicates that the stress proteome is maintained during the 1-h post stress period (Figure 5D). In the pairwise comparison of the stressed and recovered proteomes, 37°C and 37°C-recovered correlated better (R = 0.72) than 42°C and 42°C-recovered (R = 0.57). The correlation of the recovered proteome with the ribosome profiling data at 37°C was R = 0.46. We observed that the recovered proteome at 42°C correlated better with the translatome under stress (R = 0.53), indicating that at severe stress the response is slightly delayed. Notably, at 37°C and 42°C, mRNA levels shift back to NHS levels during recovery, as shown for *hsp12* and *hsp42*, which are strongly upregulated under stress (Figure S6). Overall, a delayed proteomic response contributes only slightly to the discrepancy between the transcriptome and the proteome.

### Proteolysis Is a Key Determinant Shaping the HSR

In the 2D-enriched comparison (Cox and Mann, 2012) of our proteome and translatome data, the downregulated protein categories can be summarized by translation (Figures S4B and S4C). Besides proteins connected to protein folding and trehalose metabolism, proteins implicated in (proteasomal) degradation were upregulated. To test proteasomal degradation under heat shock, we first analyzed the ubiquitination state in heat-stressed cells compared to non-stressed cells (Figure 6A). Strikingly, global ubiquitination was strongly increased in cells stressed for 30 min at 37°C and 42°C, whereas ubiquitination at 46°C was unaffected compared to physiological conditions. This fits the proteome data obtained at 46°C, which did not hint at ubiquitin-dependent degradation. After 1-h recovery at 25°C, the ubiquitination levels of the cells incubated at 37°C and 42°C dropped again. Hence, the clearance of proteins dedicated to degradation by ubiquitination extends to the recovery phase. To check if the proteins are indeed degraded by the proteasome or if the elevated ubiquitination levels are due to decreased proteasomal activity under stress, we inhibited the proteasome with bortezomib (Samant et al., 2018; Groll et al., 2006). Performing the standard MS data analysis, we did not observe a strong effect. This conundrum is probably due to internal normalization of the MS data in MaxQuant. To overcome this, we normalized our data based on the intensities determined for histone proteins, which correlate robustly with the amount of cells (Wiśniewski et al., 2014). When the proteasome was blocked, the majority of proteins tended to be upregulated at 42°C. At 37°C, however, proteasomal inhibition was less influential (Figure S7A). To expand our analysis of the stress-dependent degradome, we blocked translation elongation with cycloheximide (CHX). Thus, degraded proteins could not be replenished anymore. After histone normalization, 550 proteins at 37°C and 242 proteins at 42°C were significantly downregulated (Figure S7B).

To check if the unchanged proteins are degraded or aggregating, we highlighted the aggregating proteins (blue dots), as well as the degraded proteins (brown dots; proteasomal degradation: brown crosses) in the scatterplots of the soluble proteome versus ribosome profiling data (Figure 6B). At 37°C, 35 of the unchanged soluble proteins were upregulated at the translational level. Two of the 35 potential target proteins were enriched in the insoluble fraction, and therefore, aggregation was compensated by translation. Thus, as expected, at 37°C aggregation processes do not play an important role. At 42°C,

(B) Pellet fractions of the yeast proteins extracts collected after 30 min of the respective heat stress kinetics were analyzed by LFQ-MS. Measurements were conducted in biological triplicates. For the volcano plots, a two-sample t test with FDR < 0.05 was applied. Significantly pellet-enriched proteins are colored in dark blue.

(C) Comparison of the soluble proteome after 30 min at 46°C with the corresponding total proteome measurement. The dark blue box highlights aggregating proteins, and the brown box degraded proteins. Green box: unchanged proteins (R, Pearson correlation).

(D) Correlation of the stress and post-stress proteome. The cells were stressed for 30 min at 37°C and 42°C. Subsequently, the cells were recovered for 1 h at 25°C and the soluble proteome measured by LFQ-MS. Red box: upregulated proteins, green box: unchanged proteins, blue box: downregulated proteins (R, Pearson correlation). Recovery measurements at the mRNA level are shown in Figure S6.

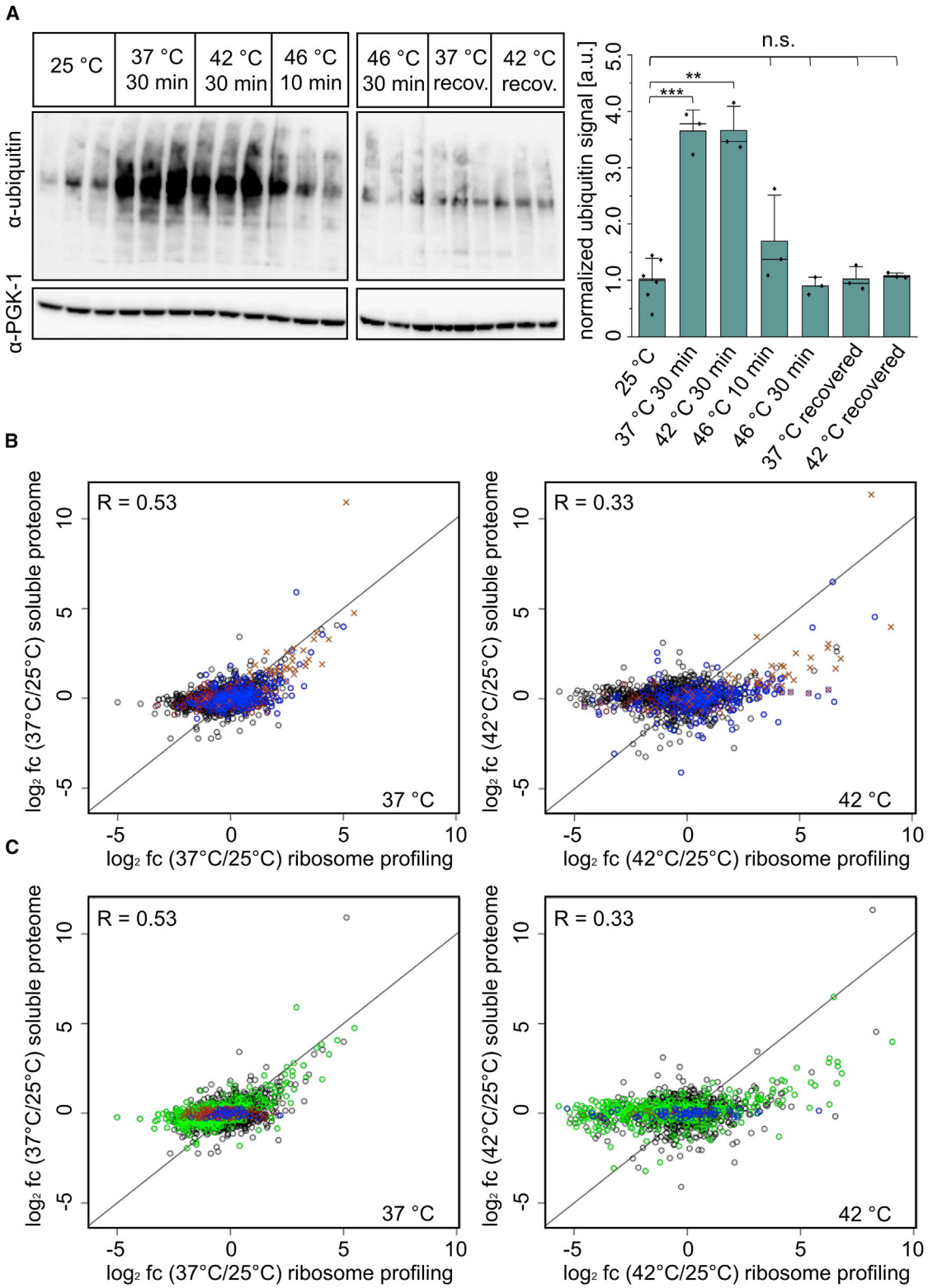


**Figure 6. Maintenance of the Proteostasis by Balancing Stress-Induced Degradation and Aggregation**

(A) Ubiquitination under stress and during recovery (from 37°C and 42°C) was analyzed by western blot. For the analysis of the ubiquitination state under stress, the same samples as for the soluble LFQ-MS were used. PGK-1 served as the loading control. Each condition was measured in biological triplicates. Data were

*(legend continued on next page)*

however, we found 72 proteins that were unchanged in the supernatant and upregulated in the ribosome profiling experiment. For 17 proteins, upregulation at the translational level compensated their aggregation and kept the amount of soluble protein constant (Figure 6B). For the other proteins with upregulated translation and unchanged soluble protein level, protein aggregation does not seem to be the major determinant. Here, proteolysis may play a role. Ten proteins at 37°C and 5 proteins at 42°C show both increased translation and increased degradation, which leads to constant levels in the soluble fraction (Figure 6B). Unfortunately, not all of the target proteins with $|\log_2 \text{fc(supernatant)}| < 0.3$ (unchanged) and $\log_2 \text{fc(RP)} > 1$ (upregulated) were found in the aggregation and degradation LFQ-MS measurements. If we narrow down the analysis to the proteins that were found in the aggregation, CHX chase, and soluble LFQ-MS measurements, we are able to show for 8 of 14 proteins at 37°C and 17 of 52 at 42°C that upregulated translation compensates their degradation and aggregation under stress and ensures a constant soluble protein pool.

Summarizing, degradation and aggregation, together with a delay of the proteomic response, explain the weak correlation of the transcriptome and the proteome. Additionally, the protein buffering effect has to be considered. Notably, the protein levels of numerous downregulated mRNAs are relatively high, which possibly explains why they are unchanged at the proteomic level (Figure 6C; green dots).

## DISCUSSION

The conceptual understanding of the HSR as a proxy for the ability of organisms to adapt to proteotoxic conditions has been focused on the role of molecular chaperones as the protective machinery. This left the vast majority of genes whose transcription is upregulated upon stress as uncharted territory. Our study, which follows the HSR from the changes in the transcriptome by the translatome to the proteome, reveals that it has three different branches. The chaperone and protection branch orchestrate a powerful machinery, which prevents and repairs conformational damage in proteins. The second branch is of anaplerotic character: by the increased expression of a large number of proteins, it guarantees constant protein levels for important metabolic processes under stress conditions and, thus, counterbalances increased degradation as well as aggregation (Figure 7). Without this regulatory compensation, the protein levels of many genes would decrease upon heat shock. Higher temperatures activate the third branch, phase transition and aggregation, followed by a regulatory shutdown of translation and growth.

Our results further suggest a modular organized HSR in which different temperatures and the severity of the damage trigger different modules. At 37°C the upregulation of molecular chaperones and metabolic processes is the predominant countermeasure, whereas at 42°C effects on translation become visible and aggregation of translation initiation factors sets in. At 46°C, the cell's efforts seem to shift to guarantee survival by the sequestration of proteins involved in translation and, hence, a shutdown of translation. We did not find specific (structural) determinants, which lead to aggregation or degradation. This issue might be addressed with limited proteolysis coupled to MS (Schopper et al., 2017).

At the transcriptomic level at a given temperature, the HSR in yeast is multi-staged, which requires a specific kinetic coordination. In yeast, the different transcription kinetics are best described with a continuum of waves of expression whereby the threshold between early and late is rather arbitrary (Figure 1B). The mechanism behind this regulatory system, which has also been shown to occur in mammalian cells (Mahat et al., 2016), remains to be determined.

During the HSR, many transcripts were reduced in their transcription. The hypothesis that the main reason for downregulation at the mRNA level is to avoid competition at the ribosome, with mRNAs coding for stress-resistance (Lee et al., 2011), is compatible with our data. Our mathematic modeling showed that protein and mRNA copies, their half-lives, and the changes in translation initiation are important parameters. However, only in combination with altered degradation or aggregation was an excellent correlation between simulated and measured changes obtained. Experimentally, we could prove that, depending on the temperature, at least 30%–50% of the upregulated genes serve to counteract aggregation and degradation and keep the respective protein levels unchanged. Thus, unexpectedly, a large part of the HSR is of anaplerotic character.

An additional surprising finding was the cellular reaction to mild heat stress (37°C). Here, the stress protective program is very efficient, and we hardly observed evidence for aggregation or decreased translation. The stress response even slightly boosted cell growth and protein biosynthesis, although protein turnover due to degradation was already increased. Thus, our data imply that a genetically driven, stress-responsive program is initiated before it is fully needed, potentially to prepare the cell for more detrimental conditions, which is in agreement with the concept of thermotolerance (Sanchez and Lindquist, 1990). The fact that the mRNA levels shift back to non-stress levels upon exposure to 37°C for increased time corroborates this hypothesis. At this temperature, phase transition does not play a regulatory role.

The aggregation of factors involved in translation represents a secondary response at 42°C and above, which ensures cell survival. This goes along with a shutdown of translation, growth, and reproduction (Figure S5B; Franzmann et al., 2018; Triandafillou

normalized on the mean ubiquitination measured at 25°C. The mean value, standard deviation, and median (black line) are shown in the bar plot. Two-sample t tests were performed to estimate the significance (N.s.: $p > 0.05$; *$p < 0.05$; **$p < 0.01$; ***$p < 0.001$) of the changes.

(B) Comparison of soluble LFQ-MS and ribosome profiling fcs after 30 min at 37°C and 42°C. Proteins that were degraded in the CHX chase experiment and unchanged in the supernatant were highlighted in brown. Upregulation in the bortezomib MS measurement is indicated by crosses. The proteins that were aggregating and unchanged in the supernatant according to LFQ-MS were highlighted in dark blue. Proteins were considered to be changed if $|\log_2 \text{fc}| > 1$ and unchanged if $|\log_2 \text{fc}| < 0.3$ (R, Pearson correlation). Volcano plots corresponding to the bortezomib and CHX chase experiment are shown in Figure S7.

(C) Comparison of soluble LFQ-MS and ribosome profiling fcs after 30 min at 37°C and 42°C. Additionally to the degraded and aggregated proteins, the 20% most abundant proteins according to Kulak et al. (2014) are indicated in green (R, Pearson correlation).

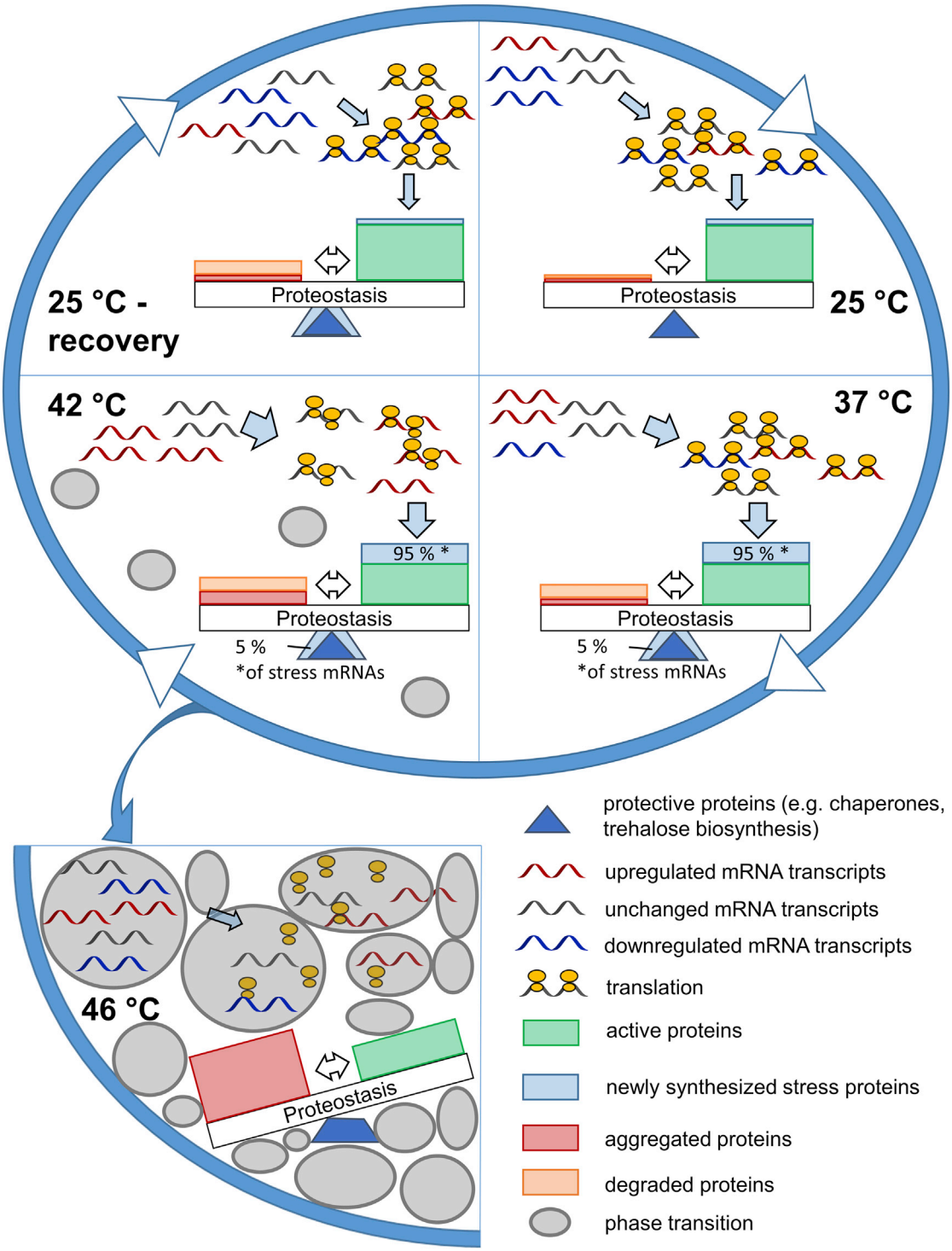


**Figure 7. Model of the HSR in Yeast**

During stress, more than 1,000 mRNAs are up- and downregulated, which is well reflected in the translational profile. The majority of the newly synthesized proteins replenishes increased protein aggregation and degradation. Approximately 10% of the upregulated genes under stress, e.g., chaperones or trehalose biosynthesis enzymes, confer stress resistance and help to balance the increased protein turnover and burden of unfolded proteins at 37°C and 42°C. During recovery, the mRNA levels and the protein turnover normalize again. Due to the stability of the Hsps, they still appear to be upregulated compared to the pre-stress time. At 46°C however, Hsps alone are not able to balance impaired protein homeostasis, and therefore, phase transition becomes necessary to freeze translation and cell growth until favorable conditions recur.

et al., 2018). In the yeast strain used, temperatures around 42°C seem to represent a thermal borderline separating the genetically driven "productive" HSR from the "dormant/life-sustaining" HSR conveyed by aggregation processes. Thus, incubation at 42°C had more detrimental outcomes for the cell. We observed a decrease in growth, even though delayed, the onset of protein aggregation processes, as well as slight deficits in TE. Importantly, the effects of proteomic downregulation are only visible after prolonged heat stress at 42°C. Shutting down *de novo* protein synthesis may be correlated to the increased recruitment of molecular chaperones to unfolding proteins during a lasting heat stress. At 46°C, we still observed a transcriptomic response, which includes the *hsp* genes; however, it was less extensive than at lower temperatures. Notably, the level reached stayed constant, indicating that no further adjustments occur. The observed shutdown of *de novo* protein synthesis implies that the cell enters a dormant phase to survive.

Notably, in an organism such as yeast, the stress response program is focused on the survival of one cell without the potentially modulating influences of non-cell-autonomous responses in multi-cellular organisms (van Oosten-Hawle and Morimoto, 2014). It will be interesting to see how the primordial-cell-autonomous response is reshaped in this context.

## STAR★METHODS

Detailed methods are provided in the online version of this paper and include the following:

- KEY RESOURCES TABLE
- LEAD CONTACT AND MATERIALS AVAILABILITY
- EXPERIMENTAL MODEL AND SUBJECT DETAILS
- METHOD DETAILS
  - Microarray
  - Ribosome profiling
  - *In vivo* $^{35}$S-Methionine incorporation
  - Cycloheximide chase
  - Inhibition of the proteasome with bortezomib
  - Genomic manipulation of *S. cerevisiae*
  - Western Blots
  - Quantitative reverse transcription PCR
  - Fluorescence microscopy
  - Scanning electron microscopy (SEM)
  - SILAC
  - Sample preparation for LFQ LC-MS/MS
  - Tryptic digest and desalting
  - MS/MS measurement
  - Data analysis
  - GO Enrichment
  - Ribosome occupancy
  - Modeling
- QUANTIFICATION AND STATISTICAL ANALYSIS
- DATA AND CODE AVAILABILITY

## SUPPLEMENTAL INFORMATION

Supplemental Information can be found online at https://doi.org/10.1016/j.celrep.2019.11.109.

## ACKNOWLEDGMENTS

We thank Florian H. Schopf and Maximilian M. Biebl for their help with the radioactive chase experiments; Miriam Güra, Maria-Teresa Mühlhofer, and Rahel Piltz for experimental support; Katja Bäuml for technical assistance with the MS measurements; Stefan Krebs for next-generation sequencing (NGS); and Bettina Richter for scanning electron microscopy (SEM) measurements. Furthermore, we are indebted to Simon Alberti for sharing his DED1-GFP constructs with us, as well as to Florian H. Schopf for his PAB1-GFP strain. This work was supported by CIPSM and SFB 1035 A06. M.M. was supported by a fellowship of the "Studienstiftung des deutschen Volkes." Bioinformatic analyses have been supported by SFB1123 Z2.

## AUTHOR CONTRIBUTIONS

M.M. and C.G.S. performed the experiments. E.K. performed the SILAC measurements. N.C.B. and S.A.S. planned and supervised the MS measurements. M.M. and N.B. processed the MS data. E.B. and G.C. processed the data, analyzed the ribosome stalling, and performed the modeling. R.Z. supervised the bioinformatic analyses. M.H. and J.B. planed and supervised the biochemical and cell biological experiments and analyses. M.M., E.B., C.G.S., G.C., M.H., R.Z., and J.B. evaluated the data. M.M., E.B., C.G.S., M.H., R.Z., and J.B. wrote the manuscript.

## DECLARATION OF INTERESTS

The authors declare no competing interests.

Received: August 5, 2019
Revised: November 22, 2019
Accepted: November 26, 2019
Published: December 24, 2019

## REFERENCES

Alberti, S. (2012). Molecular mechanisms of spatial protein quality control. Prion *6*, 437–442.

Ammar, C., Gruber, M., Csaba, G., and Zimmer, R. (2019). MS-Empire utilizes peptide-level noise distributions for ultra sensitive detection of differentially expressed proteins. Molecular & Cellular Proteomics *mcp.RA119.001509*.

Ashburner, M., Ball, C.A., Blake, J.A., Botstein, D., Butler, H., Cherry, J.M., Davis, A.P., Dolinski, K., Dwight, S.S., Eppig, J.T., et al.; The Gene Ontology Consortium (2000). Gene ontology: tool for the unification of biology. Nat. Genet. *25*, 25–29.

Belle, A., Tanay, A., Bitincka, L., Shamir, R., and O'shea, E.K. (2006). Quantification of protein half-lives in the budding yeast proteome. Proc. Natl. Acad. Sci. USA *103*, 13004–13009.

Benjamini, Y., and Hochberg, Y. (1995). Controlling the False Discovery Rate: A Practical and Powerful Approach to Multiple Testing. J R Stat. Soc. Series B Stat. Methodol. *57*, 289–300.

Bolstad, B.M., Irizarry, R.A., Astrand, M., and Speed, T.P. (2003). A comparison of normalization methods for high density oligonucleotide array data based on variance and bias. Bioinformatics *19*, 185–193.

Cherkasov, V., Grousl, T., Theer, P., Vainshtein, Y., Gläßer, C., Mongis, C., Kramer, G., Stoecklin, G., Knop, M., Mogk, A., and Bukau, B. (2015). Systemic control of protein synthesis through sequestration of translation and ribosome biogenesis factors during severe heat stress. FEBS Lett. *589*, 3654–3664.

Collart, M.A., and Oliviero, S. (2001). Preparation of yeast RNA. Curr. Protoc. Mol. Biol. *Chapter 13*, Unit13.12.

Conlin, L.K., and Nelson, H.C.M. (2007). The Natural Osmolyte Trehalose Is a Positive Regulator of the Heat-Induced Activity of Yeast Heat Shock Transcription Factor. Mol. Cell Biol. *27*, 1505–1515.

Cox, J., and Mann, M. (2008). MaxQuant enables high peptide identification rates, individualized p.p.b.-range mass accuracies and proteome-wide protein quantification. Nat. Biotechnol. *26*, 1367–1372.

Cox, J., and Mann, M. (2012). 1D and 2D annotation enrichment: a statistical method integrating quantitative proteomics with complementary high-throughput data. BMC Bioinformatics *13*, S12.

Cox, J., Hein, M.Y., Luber, C.A., Paron, I., Nagaraj, N., and Mann, M. (2014). Accurate proteome-wide label-free quantification by delayed normalization and maximal peptide ratio extraction, termed MaxLFQ. Mol. Cell. Proteomics *13*, 2513–2526.

Dobin, A., Davis, C.A., Schlesinger, F., Drenkow, J., Zaleski, C., Jha, S., Batut, P., Chaisson, M., and Gingeras, T.R. (2013). STAR: ultrafast universal RNA-seq aligner. Bioinformatics *29*, 15–21.

Edgar, R., Domrachev, M., and Lash, A.E. (2002). Gene Expression Omnibus: NCBI gene expression and hybridization array data repository. Nucleic Acids Res. *30*, 207–210.

Eisen, M.B., Spellman, P.T., Brown, P.O., and Botstein, D. (1998). Cluster analysis and display of genome-wide expression patterns. Proc. Natl. Acad. Sci. USA *95*, 14863–14868.

Erhard, F., and Zimmer, R. (2015). Count ratio model reveals bias affecting NGS fold changes. Nucleic Acids Res. *43*, e136.

Erhard, F., Halenius, A., Zimmermann, C., L'Hernault, A., Kowalewski, D.J., Weekes, M.P., Stevanovic, S., Zimmer, R., and Dölken, L. (2018). Improved Ribo-seq enables identification of cryptic translation events. Nat. Methods *15*, 363–366.

Esposito, A.M., and Kinzy, T.G. (2014). In vivo [35S]-methionine incorporation. Methods Enzymol. *536*, 55–64.

Franzmann, Jahnel, T.M., Pozniakovsky, M., Mahamid, J.A., Holehouse, A.S., Nüske, E., Richter, D., Baumeister, W., Grill, S.W., Pappu, R.V., et al. (2018). Phase separation of a yeast prion protein promotes cellular fitness. Science *359*, eaao5654.

Gasch, A.P., Spellman, P.T., Kao, C.M., Carmel-Harel, O., Eisen, M.B., Storz, G., Botstein, D., and Brown, P.O. (2000). Genomic expression programs in the response of yeast cells to environmental changes. Mol. Biol. Cell *11*, 4241–4257.

Gautier, L., Cope, L., Bolstad, B.M., and Irizarry, R.A. (2004). affy—analysis of Affymetrix GeneChip data at the probe level. Bioinformatics *20*, 307–315.

Geisberg, J.V., Moqtaderi, Z., Fan, X., Ozsolak, F., and Struhl, K. (2014). Global analysis of mRNA isoform half-lives reveals stabilizing and destabilizing elements in yeast. Cell *156*, 812–824.

Gerashchenko, M.V., and Gladyshev, V.N. (2014). Translation inhibitors cause abnormalities in ribosome profiling experiments. Nucleic Acids Res. *42*, e134.

Gerashchenko, M.V., Lobanov, A.V., and Gladyshev, V.N. (2012). Genome-wide ribosome profiling reveals complex translational regulation in response to oxidative stress. Proc. Natl. Acad. Sci. USA *109*, 17394–17399.

Ghaemmaghami, S., Huh, W.K., Bower, K., Howson, R.W., Belle, A., Dephoure, N., O'Shea, E.K., and Weissman, J.S. (2003). Global analysis of protein expression in yeast. Nature *425*, 737–741.

Gibney, P.A., Schieler, A., Chen, J.C., Rabinowitz, J.D., and Botstein, D. (2015). Characterizing the in vivo role of trehalose in Saccharomyces cerevisiae using the AGT1 transporter. Proc. Natl. Acad. Sci. USA *112*, 6116–6121.

Groll, M., Berkers, C.R., Ploegh, H.L., and Ovaa, H. (2006). Crystal structure of the boronic acid-based proteasome inhibitor bortezomib in complex with the yeast 20S proteasome. Structure *14*, 451–456.

Grousl, T., Ungelenk, S., Miller, S., Ho, C.T., Khokhrina, M., Mayer, M.P., Bukau, B., and Mogk, A. (2018). A prion-like domain in Hsp42 drives chaperone-facilitated aggregation of misfolded proteins. J. Cell. Biol. *217*, 1269–1285.

Hartl, F.U., Bracher, A., and Hayer-Hartl, M. (2011). Molecular chaperones in protein folding and proteostasis. Nature *475*, 324–332.

Huang, W., Sherman, B.T., and Lempicki, R.A. (2009). Systematic and integrative analysis of large gene lists using DAVID bioinformatics resources. Nat. Protoc. *4*, 44–57.

Ingolia, N.T., Ghaemmaghami, S., Newman, J.R.S., and Weissman, J.S. (2009). Genome-Wide Analysis in Vivo of Translation with Nucleotide Resolution Using Ribosome Profiling. Science *324*, 218–223.

Ingolia, N.T., Brar, G.A., Rouskin, S., McGeachy, A.M., and Weissman, J.S. (2012). The ribosome profiling strategy for monitoring translation in vivo by deep sequencing of ribosome-protected mRNA fragments. Nat. Protoc. *7*, 1534–1550.

Itakura, A.K., Futia, R.A., and Jarosz, D.F. (2018). It Pays To Be in Phase. Biochemistry *57*, 2520–2529.

Janke, C., Magiera, M.M., Rathfelder, N., Taxis, C., Reber, S., Maekawa, H., Moreno-Borchart, A., Doenges, G., Schwob, E., Schiebel, E., and Knop, M. (2004). A versatile toolbox for PCR-based tagging of yeast genes: new fluorescent proteins, more markers and promoter substitution cassettes. Yeast *21*, 947–962.

Jarnuczak, A.F., Albornoz, M.G., Eyers, C.E., Grant, C.M., and Hubbard, S.J. (2018). A quantitative and temporal map of proteostasis during heat shock in Saccharomyces cerevisiae. Mol. Omics *14*, 37–52.

Klein, M., Swinnen, S., Thevelein, J.M., and Nevoigt, E. (2017). Glycerol metabolism and transport in yeast and fungi: established knowledge and ambiguities. Environ. Microbiol. *19*, 878–893.

Kroschwald, S., Munder, M.C., Maharana, S., Franzmann, T.M., Richter, D., Ruer, M., Hyman, A.A., and Alberti, S. (2018). Different Material States of Pub1 Condensates Define Distinct Modes of Stress Adaptation and Recovery. Cell Rep. *23*, 3327–3339.

Kulak, N.A., Pichler, G., Paron, I., Nagaraj, N., and Mann, M. (2014). Minimal, encapsulated proteomic-sample processing applied to copy-number estimation in eukaryotic cells. Nat. Methods *11*, 319–324.

Kyte, J., and Doolittle, R.F. (1982). A simple method for displaying the hydropathic character of a protein. J. Mol. Biol. *157*, 105–132.

Lee, M.V., Topper, S.E., Hubler, S.L., Hose, J., Wenger, C.D., Coon, J.J., and Gasch, A.P. (2011). A dynamic model of proteome changes reveals new roles for transcript alteration in yeast. Mol. Syst. Biol. *7*, 514.

Lindquist, S. (1986). The heat-shock response. Annu. Rev. Biochem. *55*, 1151–1191.

Lindquist, S., and Craig, E.A. (1988). The heat-shock proteins. Annu. Rev. Genet. *22*, 631–677.

Liu, Y., Beyer, A., and Aebersold, R. (2016). On the Dependency of Cellular Protein Levels on mRNA Abundance. Cell *165*, 535–550.

Mahat, D.B., Salamanca, H.H., Duarte, F.M., Danko, C.G., and Lis, J.T. (2016). Mammalian Heat Shock Response and Mechanisms Underlying Its Genome-wide Transcriptional Regulation. Mol. Cell *62*, 63–78.

Miller, S.B., Ho, C.T., Winkler, J., Khokhrina, M., Neuner, A., Mohamed, M.Y., Guilbride, D.L., Richter, K., Lisby, M., Schiebel, E., et al. (2015). Compartment-specific aggregases direct distinct nuclear and cytoplasmic aggregate deposition. EMBO J. *34*, 778–797.

Miura, F., Kawaguchi, N., Yoshida, M., Uematsu, C., Kito, K., Sakaki, Y., and Ito, T.J.B.G. (2008). Absolute quantification of the budding yeast transcriptome by means of competitive PCR between genomic and complementary DNAs. BMC Genomics *9*, 574.

Morano, K.A., Grant, C.M., and Moye-Rowley, W.S. (2012). The response to heat shock and oxidative stress in Saccharomyces cerevisiae. Genetics *190*, 1157–1195.

Perez-Riverol, Y., Csordas, A., Bai, J., Bernal-Llinares, M., Hewapathirana, S., Kundu, D.J., Inuganti, A., Griss, J., Mayer, G., Eisenacher, M., et al. (2019). The PRIDE database and related tools and resources in 2019: improving support for quantification data. Nucleic Acids Res. *47*, D442–D450.

Protter, D.S.W., and Parker, R. (2016). Principles and Properties of Stress Granules. Trends Cell Biol. *26*, 668–679.

Riback, J.A., Katanski, C.D., Kear-Scott, J.L., Pilipenko, E.V., Rojek, A.E., Sosnick, T.R., and Drummond, D.A. (2017). Stress-Triggered Phase Separation Is an Adaptive, Evolutionarily Tuned Response. Cell *168*, 1028–1040.e19.

Richter, K., Haslbeck, M., and Buchner, J. (2010). The heat shock response: life on the verge of death. Mol. Cell *40*, 253–266.

Samant, R.S., Livingston, C.M., Sontag, E.M., and Frydman, J. (2018). Distinct proteostasis circuits cooperate in nuclear and cytoplasmic protein quality control. Nature *563*, 407–411.

Sanchez, Y., and Lindquist, S.L. (1990). HSP104 required for induced thermotolerance. Science *248*, 1112–1115.

Schaffrath, R., and Stark, M.J.R. (2014). Decoding the biosynthesis and function of diphthamide, an enigmatic modification of translation elongation factor 2 (EF2). Microb. Cell *1*, 203–205.

Schindelin, J., Arganda-Carreras, I., Frise, E., Kaynig, V., Longair, M., Pietzsch, T., Preibisch, S., Rueden, C., Saalfeld, S., Schmid, B., et al. (2012). Fiji: an open-source platform for biological-image analysis. Nat. Methods *9*, 676–682.

Schopf, F.H., Huber, E.M., Dodt, C., Lopez, A., Biebl, M.M., Rutz, D.A., Mühlhofer, M., Richter, G., Madl, T., Sattler, M., et al. (2019). The Co-chaperone Cns1 and the Recruiter Protein Hgh1 Link Hsp90 to Translation Elongation via Chaperoning Elongation Factor 2. Mol. Cell *74*, 73–87.e8.

Schopper, S., Kahraman, A., Leuenberger, P., Feng, Y., Piazza, I., Müller, O., Boersema, P.J., and Picotti, P. (2017). Measuring protein structural changes on a proteome-wide scale using limited proteolysis-coupled mass spectrometry. Nat. Protoc. *12*, 2391–2410.

Shalgi, R., Hurt, J.A., Krykbaeva, I., Taipale, M., Lindquist, S., and Burge, C.B. (2013). Widespread regulation of translation by elongation pausing in heat shock. Mol. Cell *49*, 439–452.

Spector, D., Goldmann, R., and Leinwand, L. (1998). Preparative methods for scanning electron microscopy. Cells: A Laboratory Manual (Cold Spring Harbor Laboratory Press), pp. 122.1–123.27.

Tissières, A., Mitchell, H.K., and Tracy, U.M. (1974). Protein synthesis in salivary glands of Drosophila melanogaster: relation to chromosome puffs. J. Mol. Biol. *84*, 389–398.

Triandafillou, C.G., Katanski, C.D., Dinner, A.R., and Drummond, D.A. (2018). Transient intracellular acidification regulates the core transcriptional heat shock response. bioRxiv. https://doi.org/10.1101/414706.

Tyanova, S., Temu, T., Sinitcyn, P., Carlson, A., Hein, M.Y., Geiger, T., Mann, M., and Cox, J. (2016). The Perseus computational platform for comprehensive analysis of (prote)omics data. Nat. Methods *13*, 731–740.

van Oosten-Hawle, P., and Morimoto, R.I. (2014). Organismal proteostasis: role of cell-nonautonomous regulation and transcellular chaperone signaling. Genes Dev. *28*, 1533–1543.

Verghese, J., Abrams, J., Wang, Y., and Morano, K.A. (2012). Biology of the Heat Shock Response and Protein Chaperones: Budding Yeast (*Saccharomyces cerevisiae*) as a Model System. Microbiol. Mol. Biol. Rev. *76*, 115–158.

Wallace, E.W., Kear-Scott, J.L., Pilipenko, E.V., Schwartz, M.H., Laskowski, P.R., Rojek, A.E., Katanski, C.D., Riback, J.A., Dion, M.F., Franks, A.M., et al. (2015). Reversible, Specific, Active Aggregates of Endogenous Proteins Assemble upon Heat Stress. Cell *162*, 1286–1298.

Wessel, D., and Flügge, U.I. (1984). A method for the quantitative recovery of protein in dilute solution in the presence of detergents and lipids. Anal. Biochem. *138*, 141–143.

Wiśniewski, J.R., Zougman, A., Nagaraj, N., and Mann, M. (2009). Universal sample preparation method for proteome analysis. Nat. Methods *6*, 359–362.

Wiśniewski, J.R., Hein, M.Y., Cox, J., and Mann, M. (2014). A "proteomic ruler" for protein copy number and concentration estimation without spike-in standards. Mol. Cell. Proteomics *13*, 3497–3506.

## STAR★METHODS

### KEY RESOURCES TABLE

| REAGENT or RESOURCE | SOURCE | IDENTIFIER |
|---|---|---|
| Antibodies | | |
| Rabbit polyclonal anti-Ubiquitin | Enzo | Cat# ADI-SPA-200-F |
| Mouse monoclonal anti-PGK1 | Invitrogen | Cat# 459250; RRID:AB_2532235 |
| Mouse monoclonal anti-HA Tag antibody | Invitrogen | Cat# 26183; RRID:AB_10978021 |
| Rabbit polyclonal anti-CNB1 antibody serum | Pineda | N/A |
| Rabbit polyclonal anti-HCH1 antibody serum | Pineda | N/A |
| Rabbit polyclonal anti-HSP26 antibody serum | Pineda | N/A |
| Rabbit polyclonal anti-HSP104 antibody serum | Pineda | N/A |
| Rabbit polyclonal anti-GAPDH antibody | OriGene | Cat# AP21309AF-N; RRID:AB_10758142 |
| Anti-rabbit-IgG | Sigma-Aldrich | Cat# A0545; RRID: AB_257896 |
| Anti-mouse-IgG | Sigma-Aldrich | Cat# A4789; RRID: AB_258201 |
| Chemicals, Peptides and recombinant proteins | | |
| $^{35}$S methionine | Hartmann Analytics | Cat# KSM-01 |
| Cycloheximide | Sigma-Aldrich | Cat# C-7698 |
| Bortezomib | LC Laboratories | Cat# B-1408 |
| Iodoacetamide | Merck | Cat# 8.04744.0100 |
| Trypsin, sequencing grade | Promega | Cat# V5111 |
| Glutaraldehyde | Merck | Cat# 354400 |
| Critical Commercial Assays | | |
| TruSeq Ribo Profile Library Prep Kit (Yeast) | Illumina | Cat# RPYSC12116 |
| Deposited Data | | |
| MS | PRIDE database | PRIDE database: PXD014189 |
| Bortezomib MS | PRIDE database | PRIDE database: PXD016125 |
| Microarray | Gene Expression Omnibus | Gene Expression Omibus: GSE132186 |
| NGS | SRA database | SRA database: PRJNA548255 |
| Experimental Models: Organisms/Strains | | |
| WT Yeast BY4741; MATa; ura3Δ0; leu2Δ0; his3Δ1; met15Δ0 | Euroscarf | Cat# Y00000 |
| R1158 Pab1-GFP::hygNT1 | Florian Schopf | N/A |
| BY4741; MATa; ura3Δ0; leu2Δ0; his3Δ1; met15Δ0; ded1-gfp::HisMx6 | Simon Alberti | N/A |
| R1158 Met+ URA3::CMV-tTA MATa his3-1 leu2-0 MET15 | Schopf et al., 2019 | N/A |
| BY4741; MATa; ura3Δ0; leu2Δ0; his3Δ1; met15Δ0; CMK2-6HA::HisMx6 | This work | N/A |
| Software and Algorithms | | |
| MaxQuant 1.6.2.6 | MPI Biochemistry Martinsried | https://www.biochem.mpg.de/5111795/maxquant |
| Perseus 1.6.2.1 | MPI Biochemistry Martinsried | https://www.biochem.mpg.de/5111810/perseus |
| Fiji/ImageJ | Fiji developers | https://imagej.net/Fiji/Downloads |
| ChemDraw Professional 17.1 | PerkinElmer | http://www.cambridgesoft.com/ |
| OriginPro 2018b | OriginLab | https://www.originlab.com/ |
| DAVID GeneOntology Annotation (6.8) | Huang et al., 2009 | https://david.ncifcrf.gov/summary.jsp |
| Venn Plotter | VIB / UGent Bioinformatics & Evolutionary Genomics | http://bioinformatics.psb.ugent.be/webtools/Venn/ |
| ImageQuant TL | GE Healthcare | N/A |
| affy | Gautier et al., 2004 | R package from Bioconductor |

(*Continued on next page*)

*Continued*

| REAGENT or RESOURCE | SOURCE | IDENTIFIER |
|---|---|---|
| PRICE | Erhard et al., 2018 | https://github.com/erhard-lab/price |
| STAR 2.3.1z4 | Dobin et al., 2013 | http://labshare.cshl.edu/shares/gingeraslab/www-data/dobin/STAR/STARreleases/Patches/ |

## LEAD CONTACT AND MATERIALS AVAILABILITY

Further information and requests for resource and reagents should be directed to and will be fulfilled by the lead contact, Prof. Dr. Johannes Buchner (johannes.buchner@tum.de). This study did not generate new unique reagents. There are restrictions to the availability of the TruSeq Ribo Profile Library Prep Kit. It was replaced by the ARTseq Ribosome Profiling Kit.

## EXPERIMENTAL MODEL AND SUBJECT DETAILS

In this study, the yeast strain BY4741 (MATa his3D1 leu2D0 met15D0 ura3D0) obtained from Euroscarf and derivatives of it were used. The yeast strain, generated in this study, was obtained by linear transformation. Yeast cells were cultured in YPD. Cells were grown at 25°C, unless specified otherwise.

## METHOD DETAILS

### Microarray

Yeast cells (BY4741 MATa; his3D1; leu2D0; met15D0; ura3D0) were grown in 50 mL YPD (Carl Roth) from an $OD_{595}$ of 0.2 to an $OD_{595}$ of 0.8 at 25°C before submitting the cells to thermal stress (37°C, 42°C and 46°C) in a water bath. Subsequently, the cells were harvested (1 min, 4200 x g, 4°C) and washed one time with 25 mL ice cold $H_2O$. The cells were pelleted (1 min, 4000 x g, 4°C) and the pellets shock frozen in liquid $N_2$. Sample processing was performed at an Affymetrix Service Provider and Core Facility, ''KFB - Center of Excellence for Fluorescent Bioanalytics'' (Regensburg, Germany). The chips enable the analysis of the transcriptional levels of 5,717 genes of *S. cerevisiae*. Biological triplicates for the non-stressed cells all time points at 37°C. All time points at 42°C and 46°C were measured in biological duplicates.

### Ribosome profiling

Ribosome profiling experiments were performed using the TruSeq RiboProfile (Yeast) Kit (Illumina). Yeast cells (BY4741) were grown in 500 mL YPD from an $OD_{595}$ of 0.1 to an $OD_{595}$ of 0.8 before submitting the cells to thermal stress in a water bath. Before harvesting the cells 1 mL 50 mg/ml cycloheximide (in ethanol) was added and the cells were incubated for another two minutes at RT to ''freeze'' protein biosynthesis. Subsequently, the cells were harvested (2 min, 7000 rpm, 4°C) and washed one time with 30 mL cold wash buffer (150 mM KCl; 40 mM HEPES pH 7.4; 2 mM EDTA; 2 min 4000 x g). The cells were resuspended in 3 mL yeast lysis buffer (1x polysome buffer, 1% Triton X-100, 100 μg/ml cycloheximide) and lysed as described in the kit protocol. For RNA footprinting 15 $U/A_{260}$ of 100 U/μL RNase I (Ambion) were added to 200 μL of the cell lysate. The reactions were incubated at RT and shaken at 350 rpm. After 1 h the reactions were stopped by the addition of 10 μL 20 U/μL SUPERaseIn RNase Inhibitor (Illumina) and the samples chilled on ice until separation via MicroSpin S-400 columns. After purification of the ribosome protected fragments (RPFs), rRNA was depleted according to the Ribo-Zero Magnetic Gold Kit (Illumina) procedure. Subsequently, the RPFs were gel-purified with 15% TBE/Urea gels (life technologies) and excised from the gel. For RNA extraction, the gel slices were transferred into a 0.5 mL Eppendorf tube with holes punched into the bottom and centrifuged into 1.5 mL Eppendorf tubes (ca. 5 min at 12000 x g). The shredded gel slices were suspended in 442 μL 0.45 M ammonium acetate, 0.045% SDS solution and rocked at RT for 3-4 h. Then the gel was removed by filtration over centrifugal filters (0.22 μm, Merck Millipore), 700 μL of 100% Isopropanol and 2 μL Glycogen solution (Illumina) were added and the RNA precipitated at −20°C overnight. Fragmentation of the total RNA samples, end repair, 3′ adaptor ligation, reverse transcription cDNA circularization and PCR were performed as described in the TruSeq RiboProfile Kit. The libraries were sequenced on a HiSeq1500 sequencer (Illumina).

### *In vivo* $^{35}$S-Methionine incorporation

To measure *de novo* protein biosynthesis a modified protocol described previously was used (Schopf et al., 2019; Esposito and Kinzy, 2014). Cultures of methionine prototroph R1158 (URA3::CMV-tTA MATa his3-1 leu2-0 MET15) yeast cells were grown in 5 mL CSM (-Met) over night. The cells were diluted in 50 mL CSM and again grown overnight at 30°C. On the next day, the cells were inoculated to an $OD_{595}$ of 0.2 and grown to $OD_{595}$ 0.8. Subsequently, the cells were resuspended in fresh CSM at a concentration of 1 $OD_{595}$/ml. 7 μL methionine mix (6 μL 10 mM cold methionine + 1 μL $^{35}$S-methionine; Hartmann-Analytic) were added to 1 mL cell suspension. As a growth control, parallel cultures with 7 μL 10 mM cold methionine were prepared. The cells were stressed at 37°C, 42°C and 46°C for 90 min in a thermoblock (Eppendorf) and samples taken after 10, 30, 60 and 90 min. Additionally,

90 min recovery were measured. After the heat stress 1 μL of 100 mg/ml cycloheximide (in ethanol) was added to stop translation. 1 OD was harvested and the cells were washed two times with 1 mL water + 100 μg/ml CHX. Then 400 μL 0.1 M NaOH were added to the cells and incubated for 3 min at RT. The cells were spun down once more at full speed and the supernatant discarded. Finally, the cells were resuspended in 25 μL 2.5x Laemmli buffer (5% SDS (w/v), 25% glycerol (v/v), 150 mM Tris/HCl, pH 6.8, 0.025% bromophenol blue (w/v), 2.5% (v/v) 2-mercaptoethanol) and 15 μL of the sample were loaded on a 4%–20% gradient gel (Serva). The gels were run at 25 mA constant current until the front exited the gels. The gels were placed onto a ceramic plate and wrapped with plastic wrap and autoradiography was analyzed with a Typhoon Scanner (GE LifeSciences). Densitometric analysis was performed with the ImageQuantTL Software (GE Healthcare) and the intensities normalized to 1 h at 25°C. In all our experiments, we did not notice a negative effect of growing the cells in media without methionine and supplementing them with the amino acid directly before the measurement. Since the control cells were treated in an identical manner, it seems that potential effects of methionine deprivation on translation do not play a role.

### Cycloheximide chase

Cells were inoculated to an $OD_{595}$ of 0.2 and grown to an OD of 0.8 at 25°C in YPD. Translation was stopped by adding 100 μg/ml cycloheximide (CHX). The cells were stressed for 30 min at 37°C and 42°C. As a control, degradation under non-stress conditions was analyzed in parallel. The cells were harvested for 1 min at 4200 x g at 4°C and washed one time with 1 mL ice cold buffer $S_{CHX}$ (20 mM HEPES pH 7.4, 120 mM KCl, 2 mM EDTA, 100 μg/ml CHX; 1 min 4200 x g). The pellets flash frozen in liquid nitrogen. Cell lysis and further processing is described in the sample preparation section for LFQ MS/MS to obtain the total protein.

### Inhibition of the proteasome with bortezomib

Cells were inoculated to an $OD_{595}$ of 0.2 and grown to an OD of 0.8 at 25°C in YPD. Then, the cells were treated with 50 μM bortezomib for 1 h to inhibit the proteasome (Samant et al., 2018). Subsequently, the cells were stressed for 30 min at 37°C and 42°C. As a control, the cells kept at 25°C were used. The cells were harvested for 1 min at 4200 x g at 4°C and washed one time with 1 mL ice cold buffer S (20 mM HEPES pH 7.4, 120 mM KCl, 2 mM EDTA; 1 min 4200 x g). The pellets flash frozen in liquid nitrogen. Cell lysis and further processing is described in the sample preparation section for LFQ MS/MS to obtain the total protein.

### Genomic manipulation of *S. cerevisiae*

Genomic HA tagging was performed according to Janke et al. (Janke et al., 2004). The linear DNA construct for homologous recombination was amplified via PCR from the pYM15 vector (Janke et al., 2004). Thus, it carried a 6HA tag, as well as, a HIS3MX6 cassette. The primers that were used for C-terminal tagging of CMK2 are listed below. For the transformation, yeast cells were inoculated to an $OD_{595}$ of 0.2 and grown to an OD of 0.6 at 25°C in 50 mL YPD. The cells were harvested for 5 min at 3000 x g and washed with 25 mL water. Then, the cells were resuspended in 1 mL 0.1 M Lithiumacetate and 50 μL of the cell suspension were used for one transformation approach. The cells were again pelleted and 240 μL PEG (50% w/v), 36 μL 1 M Lithiumacetate, 6 μL ssDNA and 1 μg DNA were added. The suspension was filled to 360 μL with water, vortexed and incubated for 30 min at 30°C and subsequently 30 min at 42°C. After the heat shock, the cells were carefully sedimented for 15 s at 5200 g, 1 mL of warm YPD was added and the cells recovered for 2 h. 200 μL were plated on complete supplement media (-His) and incubated at 30°C for 2-4 days. Genomic insertion was checked via colony PCR (see primers below) and western blot.

Primers for tagging: CMK2 S2: CATTAAATATTATATACGAATTTATGTACACGAATTC AAGTCCGTAATTTAATCGATGAATTCG AGCTCG; CMK2 S3: AGACGATAGCAAGAAA ACACTGCATGATGATCGGGAGTCGAAGTCAGAAGACCGTACGCTGCAGGTCGAC; Control Primers: HA rev: AGCGTAGTCTGG GAC; CMK2 ctrl fw: AACAGGAGGTGAA TTATTTG

### Western Blots

The proteins were separated via SDS-PAGE (4%–20% gradient gel; Serva) and transferred from the gel onto nitrocellulose membranes at a current of 75 mA per gel for 2 h in a semidry electro blotting device (Biometra) using 48 mM Tris, 39 mM glycin pH 9.2, 20% methanol as transfer buffer. After the protein transfer, the membrane was incubated for 60 min in 5% w/v milk powder dissolved in PBS-T (0.05% v/v Tween-20) to avoid unspecific antibody binding on the membrane. After blocking, the membrane was incubated in the respective antibody solution (1:5000 in 2.5% w/v milk powder dissolved in PBS-T) over night at 4°C. Then the membrane was washed three times with PBS-T and treated with the secondary antibody solution (1:15000 in 2.5% w/v milk powder dissolved in PBS-T). After 2 h at RT it was washed five times à 10 min with PBS-T. The blots were treated with WesternBright ECL-Spray (Advansta) and the chemiluminescence recorded on an ImageQuant LAS 4000 system (GE Healthcare). The blots were densitometrically analyzed with the ImageQuantTL Software (GE Healthcare).

### Quantitative reverse transcription PCR

RNA isolation was carried out according to the hot phenol method published by Collart and Oliviero (2001). Concentration of the isolated RNA was checked with a Nanodrop spectrometer and the integrity with an Agilent Bioanalyzer 2100 expert (Agilent Technologies, Inc; Santa Clara, CA) and the Agilent RNA 6000 Nano Kit. qRT PCR was performed using Brilliant III Ultra-Fast SYBR Green QRT-PCR Master Mix (Agilent). 1 μL of each primer, 0.2 μL 100 mM DTT, 1 μL RT/RNase Block and 100 ng total RNA were added to 10 μL 2x SYBR Green qRT-PCR Master Mix. The reactions were brought to a volume of 20 μL with nuclease free water. After mixing,

RT PCR was executed on a Mx3000P System (Agilent) or CFX Connect Real-Time PCR detection system (BioRad) with the following parameters: Reverse transcription for 10 min at 50°C, 3 min initial denaturation at 95°C, 40 cycles with 30 s denaturation at 95°C, 30 s primer annealing and 1 min elongation at 72°C. The following primers were used. Hsp12 fw: ATGTCTGACGCAGG, Hsp12 rev: TTACTTCTTGGTTGGGT; Hsp42Delta69 fw: CTAGGATCCATGTACTACCAGTTCCCTG, Hsp42 rev: CTACTAGCGGCCGCTCA ATTTTCTACCGTAGG, RDN5-1 fw: GGTTGCGGCCA, RDN5-1 rev: AGATTGCAGCACCT, RDN18-1 fw: GGTGAAATTCTTGGATTT ATTG, RDN18-1 rev: TAATGATCCTTCCGCA

### Fluorescence microscopy

Cells with GFP tagged DED1 and PAB1 were grown to an $OD_{595}$ of 0.8 and stressed at 37°C, 42°C and 46°C for 30 min. Foci formation was analyzed under the microscope (Leica Axiovert 200 with attached Hamamatsu C4742-95 camera) with a magnification of 1600x. Images were processed with ImageJ (Schindelin et al., 2012).

### Scanning electron microscopy (SEM)

SEM was performed based on a protocol published elsewhere (Spector et al., 1998). At first yeast cells were harvested for 5 min at 4000 x g and washed one time with 500 µL PBS. Subsequently, the cell pellets were resuspended in 2.5% glutaraldehyde (in PBS) and incubated 1 h at room temperature under gentle shaking. The cells were pelleted again and washed once more with PBS. Finally, the cells were resuspended in 300 µL PBS and 30 µL were distributed on a Thermanox® Plastic Coverslip (ThermoFisher Scientific) and incubated for 1-2 min at room temperature. The slides were washed in a Petri dish with 7.5 mL 50% ethanol, followed by washing steps with 7.5 mL 70% ethanol, 7.5 mL 80% ethanol, 7.5 mL 95% ethanol and three more with 7.5 mL 100% ethanol. Then, the slides were dried overnight under vacuum. Before microscopy, the cells were gold sputtered. SEM was performed with a JEOL 5900 LV microscope (JEOL, Eching, Germany). Pictures of the cells were taken at a constant voltage of 20 kV and a spot size of 20 nm at different magnifications.

### SILAC

SILAC data were used for creating the mathematical model. Labeling of yeast cultures was carried out by Stable Isotope Labeling with Amino Acids in Cell Culture (SILAC). Fresh overnight cultures of the SILAC compatible yeast strain YAL6B was grown in CSM-Arg/-Lys medium, supplemented with 100 µg/ml of Lys0 or Arg0. This culture was used to inoculate 50 mL of CSM-Arg/-Lys medium, supplemented with the respective combination of heavy-atom labeled L-Lysine-4,4,5,5-D4 (Lys4), L-Lysine-U-13C6-U-15N2 (Lys8), L-Arginine-13C6 (Arg6) and L-Arginine-U-13C6-U-15N4 (Arg10) using the following combinations: R0K0, R6K4 and R10K8. The following incubation occurred overnight (14 h) at 25°C and 130 rpm for full metabolic incorporation of the label into the proteome. This fresh overnight-culture was used to inoculate two 50 mL flasks of fresh, labeled SILAC-medium to an $OD_{595}$ = 0.25. Cultures were incubated until $OD_{595}$ = 2.0 (mid-logarithmic growth phase). At this point, control cultures were left to incubate at 25°C, while heat-shock cultures were shifted to 37°C or 42°C in a water bath. The cells were incubated for either 10 min or 30 min at 130 rpm. Next, the cells were harvested by centrifugation at 4°C and 4200 x g for two minutes, and washed once in lysis buffer (40 mM HEPES, pH 7.5, 150 mM KCl, 2 mM EDTA, 20 mM NaF, 5 mM $Na_3VO_4$, 2x MixFY (AEBSF/Aprotinin/Leupeptin/E-64/EDTA). After resuspension in 9 mL of lysis buffer, yeast cells were distributed into ten 1.5 mL reaction tubes for each labeling condition. Cells were disrupted using glass beads (r = 0.5 mm) in the bead mill with three intervals of two minutes, at a frequency of 30 $s^{-1}$. Between lysis steps, short cooling on ice occurred. After centrifugation (16000 x g, 2 min, 4°C), the supernatant of the lysate was drawn off and joined in one 15 mL falcon tube for each condition. Protein concentration was determined threefold using a BCA assay (Pierce). The lysates were flash-frozen in liquid nitrogen and stored at −80°C.

### Sample preparation for LFQ LC-MS/MS

50 mL cultures were inoculated to an $OD_{595}$ = 0.2 and grown at 25°C until an OD of 0.8 was reached. The cells were heat stressed for 30 min at 37°C and 42°C in a water bath, respectively. For measurement of recovery, the cells were shifted back to 25°C for 60 min. The cells were harvested for 1 min at 4200 x g and the samples prepared on the basis of the protocol published by Wallace et al. (2015). The cell pellets were washed one time in 1 mL ice-cold Buffer $S_0$ (20 mM HEPES pH 7.4, 120 mM KCl, 2 mM EDTA) and the pellets flash frozen. On the next day, the pellets were resuspended in 150 µL Buffer S (Buffer $S_0$, 0.5 mM DTT, 1:100 protease inhibitor MixFY (Serva), 1 mM PMSF) and divided in half. 75 µL ("1st aliquot") became the total protein sample (T) to which 500 µL Buffer T (20 mM HEPES pH 7.4, 150 mM NaCl, 5 mM EDTA, 3% (m/v) sodium dodecyl sulfate (SDS), 2 mM dithiothreitol (DTT), 10 µM PMSF, 1:1000 protease inhibitor MixFY) were added. The tubes were sealed with adhesive tape and the cells were lysed by boiling for 20 minutes at 95°C and 1000 rpm in a thermal incubator. To remove the debris, the cells were centrifuged for 1 min at 5500 x g and the supernatant flash frozen until further usage. The second aliquot was flash frozen in liquid nitrogen was lysed in a mixer mill (Retsch) with prechilled 9 mm stainless steel balls (4 x 90s at 30 Hz). Between the cycles, the tubes were chilled in liquid nitrogen. 400 µL ice-cold Buffer S were added, then the thawed lysate was clarified by centrifugation for 30 seconds at 3000 x g and 4°C and the supernatant transferred to a 1.5 mL ultracentrifuge tube. To separate the insoluble from the soluble fraction the samples were centrifuged for 25 min at 41000 rpm (TLA-45; 114480 x g) and 4°C (Optima Max E Ultracentrifuge; Beckman). The aqueous fraction was designated the soluble fraction and the pellet was washed once. The remaining pellet was mixed with 500 µL Buffer P (8 M Urea, 20 mM HEPES pH 7.4, 150 mM NaCl, 2 mM EDTA, 2% (m/v) SDS, 2 mM DTT, 10 µM PMSF, 1:1000 protease inhibitor MixFY) by

vigorous shaking in a table top thermal incubator (Eppendorf) for 30 minutes. Remaining insoluble components were pelleted for 5 minutes at 20000 x g and RT, the aqueous phase represents the "pellet fraction." Finally, the concentration of the samples was determined via BCA assay (Pierce) and the lysates flash frozen in liquid nitrogen.

### Tryptic digest and desalting

For MS analysis 250 μg protein were precipitated by the methanol-chloroform-water method as described elsewhere (Wessel and Flügge, 1984). In short: 600 μL methanol were added to 160 μL protein sample. The emulsion was centrifuged von 10 s at 14000 x g. Subsequently, 225 μL chloroform were added and centrifuged once more. Then 450 μL $H_2O$ were added, it was sonicated for 8 min and centrifuged again. The upper phase was taken off, discarded, 450 μL methanol added and centrifuged for 20 min at 14000 x g. The supernatant was completely taken off and the pellets dried on air. The pellets were dissolved in 198 μL 8 M Urea, 0.1 M Tris (pH 8.0) and 2 μL 5 M DTT were added. The samples were prepared according to the filter aided sample preparation (FASP) method (Wiśniewski et al., 2009). Briefly, the samples were loaded onto 30 kDa Microcon – 30 centrifugal filters (Merck Millipore) and centrifuged for 30 min at 14000 x g. Subsequently, the filter-collected samples were washed one time with 200 μL 8 M urea, 0.1 M Tris (30 min at 14000 x g). Then 100 μL of 50 mM iodoacetamide (IAA), 8 M Urea, 0.1 M Tris were added and mixed for 1 min at 600 rpm. Alkylation took place for 20 min at RT in the dark. The filters were centrifuged for another 20 min at 14000 x g and washed three times with 100 μL 8 M Urea, 0.1 M Tris (20 min at 14000 x g) and three more times with 50 mM ammonium bicarbonate (ABC) solution. The filters were placed into fresh collection tubes and 35 μL ABC + 5 μL 500 ng/μL Trypsin (Promega), mixed for 1 min and 600 rpm and incubated overnight at 37°C. On the next day, the filters were centrifuged again, washed with 50 μL 500 mM NaCl (15 min, 14000 x g) and the tryptic digest stopped by the addition of 0.5 μL trifluoroacetic acid (TFA). The samples were desalted with 50 mg SEP PAK (tC18) columns (Waters). At first the columns were equilibrated with 1 mL acetonitrile (ACN), 500 μL elution buffer (80% (v/v) ACN, 0.5% (v/v) formic acid (FA) and three times with 1 mL 0.1% (v/v) TFA. After loading of sample, the column was washed three times with 1 mL 0.1% (v/v) TFA and one time with 250 μL 0.5% (v/v) FA. The samples were eluted with two times 250 μL elution buffer by gravity flow and then one more time with 250 μL elution buffer with vacuum applied. The samples were dried in a speed vacuum centrifuge (Eppendorf) and the peptides stored at −20°C. For the measurement, samples were dissolved in 20 μL 1% FA and incubated for 5 min in an ultrasonic bath at RT. The solutions were filtered through 0.22 μm centrifugal filters (Merck; 2 min at 16200 x g). For the measurement, the solutions were transferred into Chromacol vials (Thermo Scientific).

### MS/MS measurement

MS analysis was performed on either an Orbitrap Fusion or a Q Exactive Plus instrument coupled to an Ultimate3000 Nano-HPLC via an electrospray easy source (all Thermo Fisher Scientific). Samples were loaded on a 2 cm PepMap RSLC C18 trap column (particles 3 μm, 100A, inner diameter 75 μm, Thermo Fisher Scientific) with 0.1% TFA and separated on a 50 cm PepMap RSLC C18 column (particles 2 μm, 100A, inner diameter 75 μm, Thermo Fisher Scientific) constantly heated at 50°C. The gradient was run from 5%–32% acetonitrile, 0.1% formic acid during a 152 min method (7 min 5%, 105 min to 22%, 10 min to 32%, 10 min to 90%, 10 min wash at 90%, 10 min equilibration at 5%) at a flow rate of 300 nL/min.

For measurements on the fusion instrument survey scans (m/z 300-1500) were acquired in the orbitrap with a resolution of 120000 at m/z 200 and the maximum injection time set to 50 ms (target value 2e5). Most intense ions of charge states 2-7 were selected for fragmentation with high-energy collisional dissociation at a collision energy of 30%. The instrument was operated in top speed mode and spectra acquired in the ion trap with the maximum injection time set to 50 ms (target value 1e4). The option to inject ions for all available parallelizable time was enabled. Dynamic exclusion of sequenced peptides was set to 60 s. Real-time mass calibration was based on internally generated fluoranthene ions. Data were acquired using Xcalibur software version 3.0sp2 (Thermo Fisher Scientific).

For measurements on the Q Exactive Plus instrument survey scans (m/z 300-1500) were acquired in the orbitrap with a resolution of 70,000 at m/z 200 and the maximum injection time set to 80 ms (target value 3e6). Data dependent HCD fragmentation scans of the 12 most intense ions of the survey scans were acquired in the orbitrap at a resolution of 17500, maximum injection time of 50 ms as well as minimum and maximum AGC targets of 5e3 and 5e4, respectively. The isolation window was set to 1.6 m /z. Unassigned, singly charged ions were excluded from the measurement, and the dynamic exclusion of peptides enabled for 60 s. The lock-mass ion 445.12002 from ambient air was used for real-time mass calibration on the Q Exactive Plus. Data were acquired using Xcalibur software version 3.1sp3 (Thermo Fisher Scientific).

### Data analysis

Quantitative analysis of the MS data was performed with MaxQuant (version 1.6.2.6) (Cox et al., 2014; Cox and Mann, 2008). The raw files were searched against the *S. cerevisiae* proteome database downloaded from UniprotDB. All files were assigned to the same fraction, only tryptic peptides were searched, cleavage sites before proline were included. Up to two missed cleavage sites were allowed as well as a peptide tolerance of 4.5 ppm. As variable modifications N-terminal acetylation and methionine oxidation were selected, as fixed modification carbamidomethylation with maximal 5 modifications per peptide. Label free quantification (LFQ) was performed with a min. ratio count of 1. Otherwise, the orbitrap instrument settings of MaxQuant were applied. Minimal peptide length was set to 7 amino acids, the maximal length was 25 amino acids. To enhance protein recovery match between

runs was applied (match time window 0.7 min; align window 20 min). The identification parameters were left preset with a protein FDR of 1%. Label min. ratio count was set to 1 and unique + razor peptides were taken into account. For the statistic validation of the results, the peptides were also searched against a reverse decoy database calculated by MaxQuant.

The processed raw data were further evaluated by Perseus (version 1.6.2.1) (Tyanova et al., 2016). The protein groups file was filtered by potential contaminant hits, hits from the reverse database and hits only identified by site. The LFQ intensities were $\log_2$ transformed, grouped into replicates and the rows filtered on 3 valid values in each replicate group. The pellet fractions were filtered on 3 valid values in at least one group to avoid loss of proteins that are only aggregating at a distinct temperature. The MS data belonging to the CHX chase experiment were filtered on at least 2 valid values in each group to raise the number of identified proteins. If it was filtered on two valid values or 3 valid values in at least one group, the missing values were calculated from the Gaussian distribution (width: 0.3; downshift: 1.8). Volcano plots with a two-sided t test (FDR: 0.05; $S_0 = 0.1$) were plotted (Benjamini and Hochberg, 1995). A protein was considered to be significantly up- or downregulated if $|\log_2 fc| > 1$; FDR < 5% and $S_0 = 0.1$. For the comparisons with the transcriptome and translatome data, we used the fold change. We consider a gene/protein to be *changed* if $|\log_2 fc| > 1$ and *unchanged* if $|\log_2 fc| < 0.3$. Pearson correlations were calculated and 2D enrichment plots were visualized with Perseus. The CHX chase and the Bortezomib LFQ data were additionally histone normalized using the mean protein level of HHT1, HTB2 and HHF1 or HTZ1, HHF1 and HHO1, respectively, to correct for the internal normalization used by MaxQuant.

Microarray data was processed using the affy R package (Gautier et al., 2004; Bolstad et al., 2003) and summarized by RMA (Bolstad et al., 2003). Depending on the number of replicates different approaches were used to define the (significantly) changed genes. For the measurements at 37°C, 3 replicates are available and a two-sided t test is performed. Genes with Benjamini-Hochberg corrected p value < 0.05 and $|\log_2 fc| > 1$ are considered significantly changed. For the other temperatures only 2 replicates per condition are available. Here, we calculated all replicate combination fold changes and considered a gene to be robustly changed when all these $\log_2$ fold changes were above or below 1.

The ribosome profiling data was mapped with STAR (Dobin et al., 2013). Counts were derived from reads assigned to codons by PRICE (Erhard et al., 2018) The fold changes and their significance was calculated with EmpiRe (Ammar et al., 2019). As there is no "obvious" way to derive fold changes for the cases where counts were observed only in replicates of one condition but not in the other we discard them in the scatter plots. Genes in the ribosome profiling sequencing data are defined to be significant if the multiple testing corrected p-value derived from EmpiRe is < 0.05 (Ammar et al., 2019) and the corresponding change is $|\log_2 fc| > 1$.

To calculate the translation efficiency (TE) the mRNA and ribosome profiling measurements were made comparable by the median normalization of EmpiRe.

### GO Enrichment

For GO term enrichment analysis, we used the DAVID tool (Huang et al., 2009; Ashburner et al., 2000) or the UniProt annotation Table (2015) downloaded from the Perseus GitHub (for the 2D enrichment plots) (https://datashare.biochem.mpg.de/s/qe1IqcKbz2j2Ruf). The resulting p values are multiple testing corrected using the method of Benjamini-Hochberg and GO processes with a p value below 0.05 were reported as enriched (Ashburner et al., 2000; Benjamini and Hochberg, 1995).

### Ribosome occupancy

In contrast to prior methods to identify stalled transcripts in ribosome profiling data, our method is designed to find condition dependent stalled transcripts (i.e., only transcripts that were stalled upon heat stress) and is able to integrate replicate measurements. It identifies both the optimal stalling point (i.e., the position of the transcript at which the ribosomes are stalled) and a measure for the stalling strength. In order to focus on condition dependent stalling events we chose a differential setup, for which we extend the model of the local fold change method (Erhard and Zimmer, 2015).

To find the optimal stalling point a log-ratio test for each transcript and each possible stalling point was performed. The test compares the model with stalling against a model without stalling. For the model without stalling, one beta-binominal distribution was fitted to the local (position-wise) fold changes between a stressed and unstressed replicate. In the stalled model two beta-binominal distributions were used to model the local fold changes of the transcript: one for the positions upstream of the stalling point and the other for the positions downstream of the stalling point. This way the log-ratio test tests whether it is better to model the fold changes by one joined distribution (no stalling) or by two separate distributions (stalling). To incorporate replicate measurements, all r possible replicate combinations were modeled this way with a separate set of beta-binominal distributions (to account for differences in library size) and combined into a joined model. This joined model thus tests the no-stalling model with r beta-binominal distributions against the stalling model with 2*r distributions. To reduce the effect of positions with many reads due to PCR bias, the read counts were down-sampled to the log value (Erhard and Zimmer, 2015) of the maximal count of the position. A log-ratio test was done for each position for each transcript and the position with the minimal p value was used as the optimal stalling point.

The p value only quantifies the confidence that there is a difference between the distributions before and after the stalling point, but not how strong the ribosomes are stalled, i.e., the size of the difference between the two distributions. Thus, we used the fold change difference distribution, i.e., the difference between the two beta-binomial distributions upstream and downstream of the optimal stalling point as the stalling strength. The advantage of keeping the complete distribution instead of summarizing it to one value (e.g., the median) is that the width of the distribution corresponds to the confidence of the measurement, which could be used to filter

unreliable measurements. In order to be able to subtract two distributions from each other, we sampled the probabilities of each distribution in regularly spaced intervals and summed up the combined probabilities for each of the resulting fold change differences. This yielded an empirical estimate of the combined distribution for each replicate combination. These replicate-pair fold change difference distributions were combined by taking the mean over the probabilities of all distributions for each sampled fold change difference. We defined a transcript to be stalled if the log-ratio test p value to define its optimal stalling point was below 0.001, the 5%-confidence interval of all replicate-pair fold change difference distributions were above 0 and the expected fold change difference is above 1.

For the hydropathy profiles, the hydrophobicity of the amino acids by Kyte and Doolittle (1982) was used to calculate the average hydrophobicity of the first 80 bases of the protein sequence of all transcripts in the corresponding group (Kyte and Doolittle, 1982). A sliding window of size 20 was used to smooth the resulting profile.

### Modeling

Lee et al. (2011), model the protein change over time by

$$P_{\rho}^{'}(t) = k_{s,\rho}(t)m_{\rho}(t) - (k_{d,\rho} + \mu(t))P_{\rho}(t)$$

where $P_{\rho}(t)$ is the amount of protein of protein $p$ at time $t$, $k_{s,\rho}(t)$the translation rate, $m_{\rho}(t)$the amount of mRNA, $k_{d,\rho}$ the decay rate and $\mu(t)$ the diffusion rate due to growth (Lee et al., 2011).

Similar to Lee et al. (2011) we used protein half-lives (Belle et al., 2006), absolute initial protein levels (Ghaemmaghami et al., 2003) and our own measurements of growth rates, ribosome profiling and protein fold changes measured by SILAC after 10 and 30 min. Given these measurements, Lee et al. (2011) could estimate the parameter $k_{s,\rho}(t)$ for each protein to fit optimally to all protein measurements. As we used ribosome profiling instead of expression data, $k_{s,\rho}(t)$ corresponds to the protein synthesis rate from ribosome bound mRNA instead of an estimated translation rate. The rate limiting step of translation is initiation so that we conclude that $k_{s,\rho}(t)$should be constant over time and should not change upon heat shock. This allowed us to calculate the protein synthesis rate $k_{s,\rho}(t)$ directly from the steady state measurements without the need to fit thousands of parameters, which is prone to overfitting.

Furthermore, this model was used to test hypotheses about additional mechanisms that influence the protein synthesis (i.e., $k_{s,p}$) or protein degradation (i.e., $k_{d,p}$). Using a parsimonious approach, we analyzed if there are groups of proteins whose protein degradation is affected similarly. For this, we divided the proteins into three groups based on their changes in the ribosome profiling data: proteins that were upregulated ($\log_2$fc > 1 in at least one time point), downregulated ($\log_2$fc < −1 in at least one time point) or unchanged. We assume that the steady state half-lives are suitable for the unchanged proteins but have to be adapted for the up- and downregulated proteins. Thus, we optimized for each of the two groups of proteins one multiplicative factor that is applied to $k_{d,p}$. This yielded a factor of 0.57 for the upregulated proteins and 1.69 for the downregulated proteins, which corresponds to increased degradation/aggregation for the proteins with increased translation and less degradation/aggregation for the proteins with decreased translation. When we used these modified half-lives in our model, there were fewer proteins with huge differences between the simulated and measured fold changes. Overall, using these modified values instead of the steady state parameters improved the fit.

Similarly to Lee et al. (2011), we also fitted individual parameters for $k_{s,p}$ and analogously also for $k_{d,p}$. Both optimizations yielded a very good correlation between the measured and predicted protein fold changes. However, due to the large number of optimized parameters (equal to the number of proteins) these two fits are likely to overfit and serve as a best-case estimate of model predictions of the actual measurements.

## QUANTIFICATION AND STATISTICAL ANALYSIS

Statistical parameters are reported in the figures and figure legends. Statistical significance was assigned by using a two-sample t test. P values below 0.05 were classified as significant (N.s.: p > 0.05; *p < 0.05; **p < 0.01; ***p < 0.001). In the bar plots the bar heights represent the mean value, the black lines the median and the error bars the standard deviation. Statistical analyses were performed using OriginPro 2018b or Perseus. For specific methods, the respective software used is mentioned in the Method Details. We define the unchanged genes/proteins as those with an absolute $\log_2$ fold change below 0.3. Even though these thresholds are arbitrary, they conservatively and robustly identify both the changed and unchanged genes/proteins. Note that there is a gap of $\log_2$ fc difference of 0.7 between 0.3 (unchanged) and 1.0 (changed) indicating that proteins in this gray zone are neither clearly changed nor unchanged.

## DATA AND CODE AVAILABILITY

The mass spectrometry proteomics data have been deposited to the ProteomeXchange Consortium via the PRIDE (Perez-Riverol et al., 2019) partner repository with the dataset identifier PRIDE database: PXD014189.

The proteome samples in which the proteasome was inhibited with bortezomib can be accessed with the identifer PRIDE database: PXD016125.

The microarray data discussed in this publication have been deposited in NCBI's Gene Expression Omnibus (Edgar et al., 2002). NCBI's Gene Expression Omnibus: GSE132186 (https://www.ncbi.nlm.nih.gov/geo/query/acc.cgi?acc=GSE132186).

The secure token for reviewer access is: yhutsmgadjohvwh.

Sequencing data are deposited at the SRA database. SRA database: PRJNA548255 (https://www.ncbi.nlm.nih.gov/sra/PRJNA548255).

All fold changes of the single RNA-seq/ ribosome profiling/ LFQ-MS measurements are available in the supplemental Excel sheet. The other datasets used for this study are available from the corresponding author upon request.